Introduction to Computational Models for Multiphase Flows

Introduction to computational models for multiphase flows

Daniele Marchisio *
Institute of Chemical Engineering
Department of Applied Science and Technology
Politecnico di Torino (Torino)
Italy

May 2021

Contents

*DISAT - Politecnico di Torino, Corso Duca degli Abruzzi 24, 10129, Torino, Italy; email: daniele.marchisio@polito.it

1 Introduction to multiphase flows

The objective of these notes is to describe the different types of multiphase flows that are typically encountered in nature and in engineering applications and the corresponding computational models that can be used for their simulation. Multiphase flows are characterized by the simultaneous presence of different phases. A first classification can be based on the number of phases present. Most multiphase systems are characterized by the presence of two phases only and they are generally referred to as two-phase flows. As depicted in Fig. 1 different types of multiphase flows are encountered, namely:

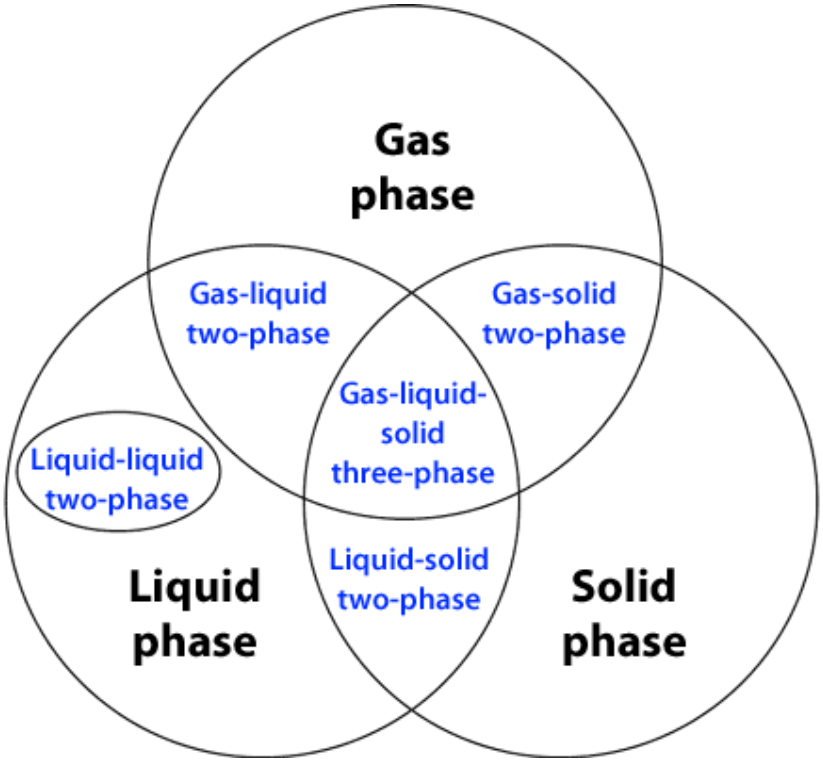

Figure 1: A possible classification of multiphase systems based on the type of phases involved.

- gas-liquid,
- gas-solid,
- liquid-solid,
- liquid-liquid.

In some cases more than two phases are present, as for example in the case of gas-liquid-solid systems, and these are referred to as three-phase flows.

This classification is not exhaustive, as in some cases multi-phase systems can be observed when three (or more) immiscibile liquids are mixed together. Another example can be the case of a gas transporting both droplets and solid particles. However with a reasonable degree of approximation what depicted in Fig. 1 can be used as a working

definition of multiphase flow. Readers interested in more details can refer to the specialized literature (Prospetti and Grétar, 2007; Marchisio and Fox, 2007; Bird et al., 1960; Clift et al., 1978; Marchisio and Fox, 2013).

Another important definition is that of *dispersed* and *separated* flows, depicted in Fig. 2. The former (i.e. dispersed) being those consisting of finite particles, droplets or bubbles distributed within a continuous phase. The latter (i.e. separated) is defined as consisting of two or more continuous streams of fluids separated by interfaces. Only gas-liquid and liquid-liquid systems can be separated. It is important to highlight that in many practical applications (such as for example during boiling flows) a system can be simultaneously dispersed and separated.

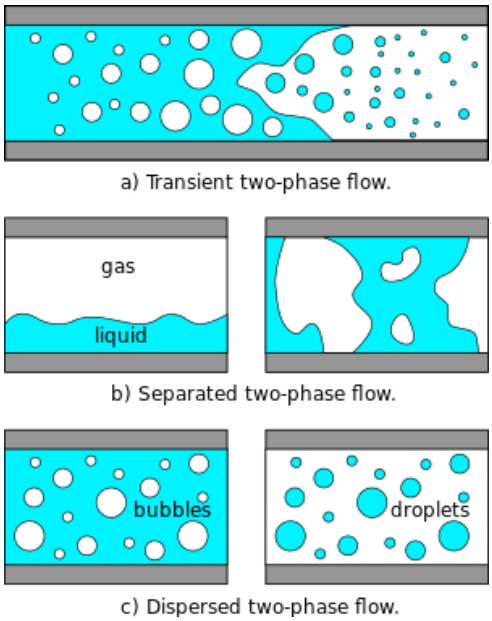

Figure 2: Sketches representing separated or dispersed multiphase flows. A dispersed system (c) is characterized by individual bubbles, droplets or solid particles. A separated flow (b) is characterized by continuous streams of the involved phases separated by an interface. It is important to highlight that in many practical applications (such as for example during boiling flows) a system can be simultaneously dispersed and separated (a).

1.1 Gas-liquid systems

Gas-liquid systems are encountered in numerous engineering applications and can be classified depending on the type of flow regimes and the type of flow structures observed, as depicted in Fig. 3 . For example, when a liquid and a gas are flowing together in a pipe and depending on the relative flow rates of the two phases different regimes are observed. For a given liquid flow rate, when the gas low rate is low, typically the gas appears in the form of individual bubbles, resulting in the so-called bubbly flow. Under these conditions the liquid can be defined as continuous phase, also referred to as primary phase, whereas gas bubbles can be defined as disperse phase, also referred to as secondary phase. When the gas flow rate is increased the resulting regimes are classified as: slug flow,

semi-annular flow and annular flow. Under these conditions it is not possible to identify a continuous phase and a disperse phase and the two phases can be locally continuous or disperse. When the gas flow rate is much larger than the liquid flow rate, phase inversion occurs and the misty flow regime is observed, in which the continuous primary phase is the gas and the disperse secondary phase is the liquid. Under these conditions the liquid appears in the form of individual droplets, which depending on their size can be classified as aerosol, although the word aerosol is also used to identify a gas carrying around small solid particles. Systems in which liquid droplets are dispersed into a continuous gas phase are also referred to as sprays.

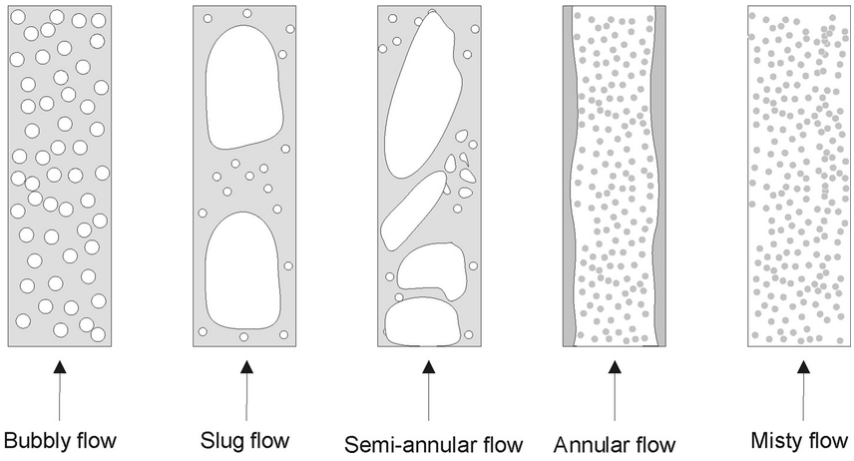

Figure 3: A possible classification of gas-liquid flows.

Engineering applications. Gas-liquid systems are omnipresent in engineering applications, such as for example in boiling flows, for energy production processes or cooling, in pipelines of the oil and gas industry, or in chemical reactors. Numerous chemical processes are conducted in reactors called bubble columns, with no moving parts, in which gas bubbles are dispersed in a liquid to promote mass and heat transfer between the two phases to conduct, under controlled conditions, chemical reactions. Other applications in the chemical industry involve gas-liquid stirred tanks, in which the contact between phases is helped by mechanical stirring. Figure 3 depicts four different reactor configurations employed for example in fermentation processes and bioreactors in general. Relevant examples can be found in the specialized literature (Li et al., 2021, 2020, 2019; Gemello et al., 2019; Shiea et al., 2019).

Misty flows are encountered in filters and separators, in which the liquid droplets are removed from the gas by using a porous medium or repeated obstacles. Sprays are very common in industrial painting, as well as in combustion processes, where a liquid fuel is atomized into small droplets that then evaporates to react with the surrounding gas phase. A typical evaporating spray is sketched in Fig. 5 together with the phenomena involved. The first atomization is called primary breakup, followed by the rupture of the droplets into smaller droplets, referred to as secondary breakup.

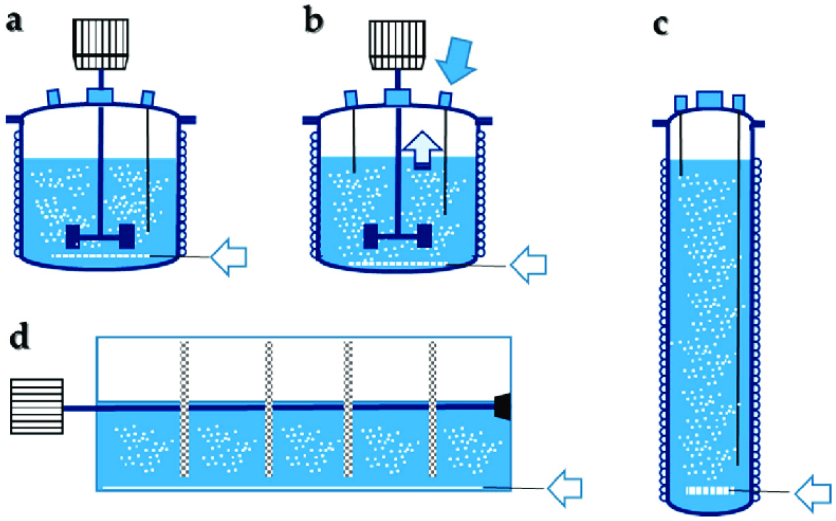

Figure 4: Four different reactor configurations for gas-liquid systems: (a,b) gas-liquid stirred tank with different feeding strategies and (c,d) bubble columns with different design options to favor the contact between phases.

1.2 Gas-solid systems

In gas-solid systems the gas phase carries around solid particles. These systems are generally always disperse, in the sense that it is always possible to identify a continuous phase, the gas, and a disperse phase, the solid particles. The solid particles typically interact with the surrounding gas phase by exchanging mass, momentum and energy, and interact with each other via collisions. Depending on the solid concentration different regimes can be identified. At low solid particle concentration collisions are not frequent and the most relevant phenomena are limited to the interaction between the solid and the gas phases. This is the so-called kinetic regime. When the solid content increases collisions are more important and dominate the dynamics of the system, resulting in the so-called collisional regime. When the solid content is further increased the enduring contacts between particles control the corresponding transport phenomena and this is called the frictional regime.

Engineering applications. Gas-solid systems are encountered in nature, when solid particles are transported by a gas flow, as for example in sand storms or vulcano's eruptions. In engineering applications gas-solid flows are common in pneumatic transport or in fluidized beds. Fluidized beds are employed in the chemical industry for combustion, polymerization and gassification processes. Figure 6 depicts what happens at increasing gas flow rates in a typical fluidized bed. At the low gas flow rate the bed of solid particles is packed and the particles remain deposited at the bottom of the reactor. When the gas flow rate is increased over a critical value, called minimal fluidization velocity, the drag force exerted on the particle is enough to suspend them in what is called the homogeneous fluidization regime. When the gas flow rate is further increased flow instabilities induce the formation of gas bubbles that grow as they rise and leave the bed, in what is called the bubbling flow regime. Further increase of the gas flow rate induces the development

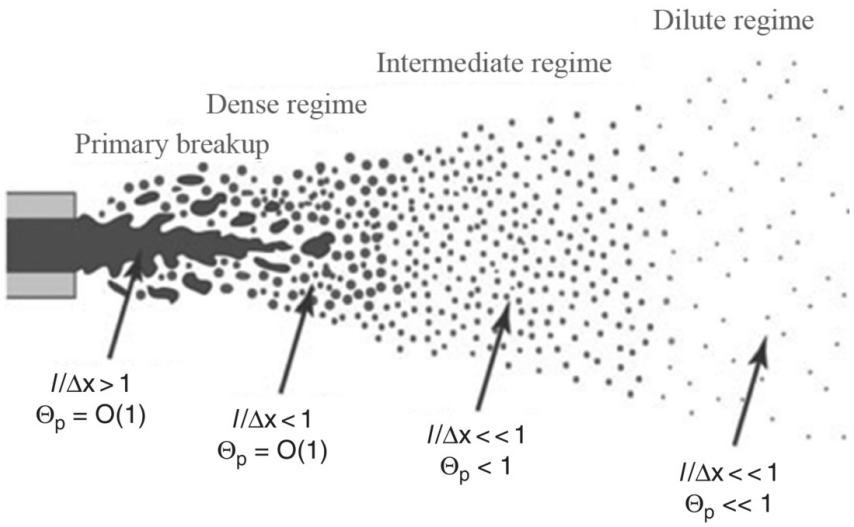

Figure 5: Sketch representing a spray and the phenomena involved in its formation, namely primary and secondary breakup.

of other flow regimes depicted in the figure. At last it can be mentioned that gas-solid granular flows are also very common in the pharmaceutical industry. Relevant examples can be found in the specialized literature (Pollack et al., 2019; Salenbauch et al., 2019).

1.3 Liquid-solid systems

In liquid-solid systems solid particles, which constitute the secondary disperse phase, are suspended in a liquid resulting in flow configurations that are very similar to those exhibited by gas-solid systems. The main difference is that here the continuous phase is a liquid, that being generally more dense and viscous of a gas, makes particle collisions less important. These flows are dominated by the interaction between the solid particles and the surrounding liquid phase and a crucial parameter is played here by the particle size. When the particle size is very small the solid particles tend to move together with the fluid and the liquid-solid system is treated as a pseudo-single phase system. For larger particle sizes inertial effects start to be important and the solid particles tend to move with their own velocity. Under these conditions the system cannot be treated as a pseudo-single phase system and other approaches are needed. To distinguish between one regime and the other a dimensionless number, the Stokes number, is typically introduced. This will be discussed later in Section 1.6.

Engineering applications. Liquid-solid flows are very frequent in nature, as in many environmental applications solid particles are transported by a liquid (typically water) in rivers, lakes and aquifers. Liquid-solid flows are also common in the chemical, pharmaceutical and food industries. One important application that is worth mentioning is crystallization, a very popular separation method. In crystallization processes solid formation is induced in a liquid by changing the solubility of a substance by displacing a solvent or by changing the temperature. Solid particle formation is governed by nucleation which can be homogeneous or heterogeneous, depending on the characteristic value of the

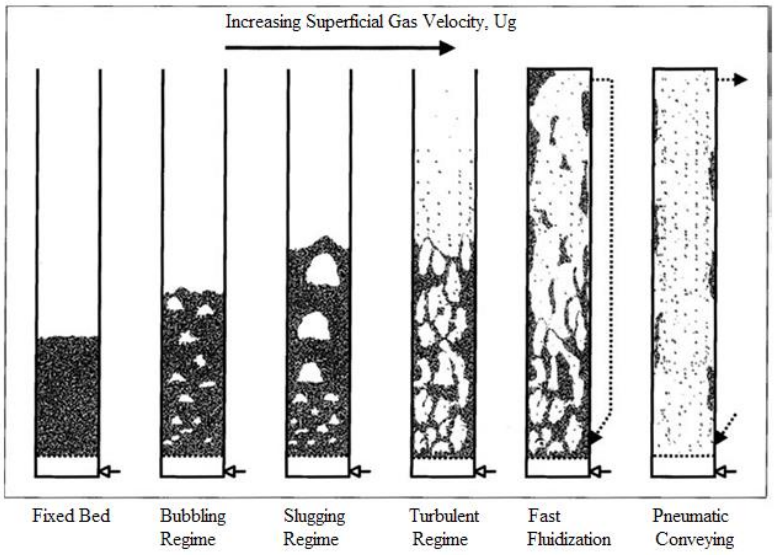

Figure 6: Fluidization regimes in fluidized beds. From left to right: fixed bed, bubbling regime, slugging regime, turbulent regime, fast fluidization and pneumatic conveying or transport.

driving force, which is known as supersaturation. After particles are formed they can grow continuously, due to the addition of single molecules of the solute, or via aggregation. During aggregation formed particles can collide and stick together forming a larger particle called aggregate or agglomerate. In a typical crystallization process, particles can also undergo breakage, due to fluid dynamics stresses or impact of the particle on a surface, either a wall of the crystallizer or the blade of an impeller. Relevant examples can be found in the specialized literature (Boccardo et al., 2019b; Frungieri et al., 2020; Marcato et al., 2021).

1.4 Liquid-liquid systems

Liquid-liquid systems are obtained when two immiscible liquids are mixed together. Most liquid-liquid systems are constituted by a polar liquid mixed with a non-polar liquid. In liquid-liquid emulsions it is always possible to identify one continuous primary phase and a secondary disperse phase, constituted by individual droplets. When the concentration, often expressed in terms of the volume fraction, of the disperse phase increases over a critical value, the disperse phase can become continuous and, viceversa, the continuous phase can become disperse. This is called phase inversion and depending on the situation this can be a wanted or unwanted situation. When surface active ingredients, such as surfactants, are added the liquid-liquid dispersion becomes stable and is often referred to as emulsion. Liquid-liquid dispersions and emulsions are often characterized by a relatively small density ratio between the disperse phase and the continuous phase. This situation leads to small, if not negligible, inertial effects, allowing for their treatment as a pseudo-single phase system. Very important is the role played by the viscosity ratio, between the disperse and continuous phases. Depending on this ratio different behaviors

are observed, especially in terms of the droplet breakage rate. Liquid-liquid dispersions and emulsions when treated as a pseudo-single phase system exhibit non-Newtonian shear thinning rheological behaviors, as well as an elastic component. These behaviors depend on the disperse phase volume fraction, as summarized in Fig. 7. When the disperse phase is dilute the rheology is dictated by the continuous phase, whereas when a critical concentration is overcome (concentrated regime) non-Newtonian shear-thinning behaviors are observed. A further increase in the disperse phase concentration leads to the formation of caged or closely-packed microstructures, resulting in an elastic component. The system remains fluid, as if a strong enough shear rate is applied the system starts flowing. In that sense emulsions are often referred to as soft matter.

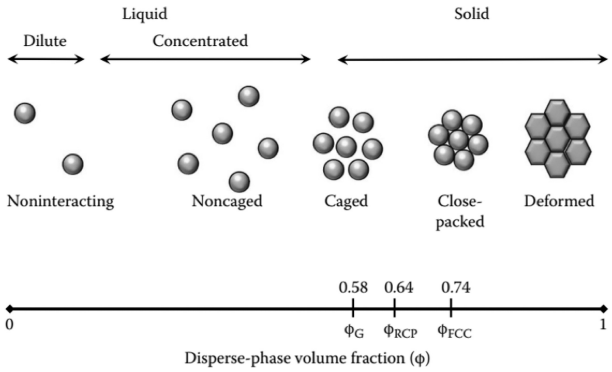

Figure 7: Rheological response observed in liquid-liquid systems and emulsions. When the disperse phase is dilute the system exhibit a Newtonian behavior. When the disperse phase concentration is increased non-Newtonian shear-thinning and elastic responses are also observed.

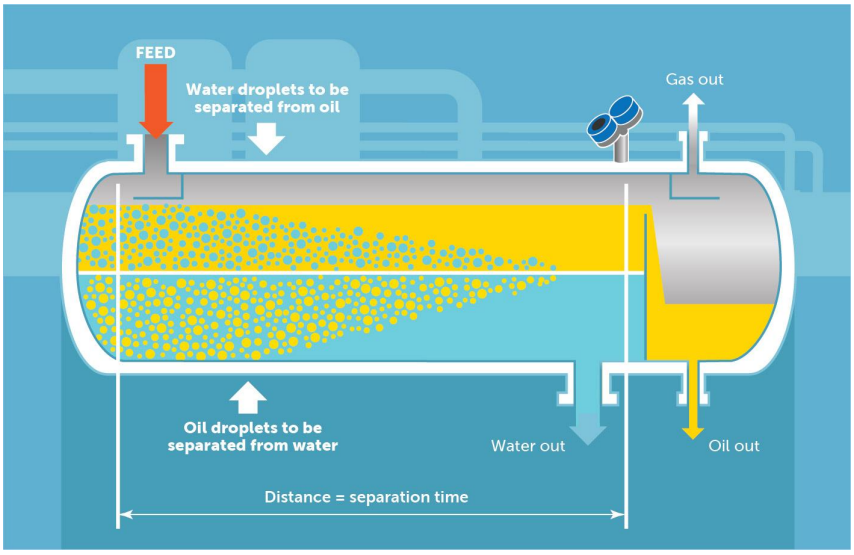

Figure 8: Typical separator for liquid-liquid dispersions employed in the oil and gas industry.

Engineering applications. Liquid-liquid systems, dispersions and emulsions are very common in the oil and gas industry. During drilling, extraction and oil recovery applications oil often ends up being mixed with water generating liquid-liquid dispersions. In order to separate the two phases, ad-hoc separators are designed and in this area the investigation of their property and features is of paramount importance. An example of such a system is reported in Fig. 8. Other interesting application areas in which emulsions are often encountered are the pharmaceutical, cosmetic and food industries. Probably the most popular food emulsion is mayonnaise. Mayonnaise is constituted by a highly concentrated dispersion of oil droplets, in an aqueous phase, stabilized by surfactants molecules contained in the egg yolk, namely proteins (e.g. apovitellenin I) and phospholipids. In industrial applications the production and fate of liquid-liquid systems is often dictated by the the dynamics of coalescence and breakup. Coalescence results from the merging of two colliding droplets, whereas breakup is the generation if two or more daughter droplets, due to the excessive deformation of one mother droplet. Both coalescence and breakup are caused by fluid flow and deformation. Relevant examples can be found in the specialized literature (Marcato et al., 2021; Castellano et al., 2019; Boccardo et al., 2019a).

1.5 Disperse and polydisperse flows

As mentioned, dispersed multiphase flows are characterized by the presence of a continuous phase, either a liquid or a gas, and a disperse phase, constituted by individual droplets, bubbles and particles. Their features are very different from separated flows, which are instead characterized by a consistent stratification of one phase over another, with large regions with only of one the two phases present. Separated flows, very important in nature, as for example in the dynamics of waves or breaking waves, are dominated by interfacial forces, active in the interface between the two phases.

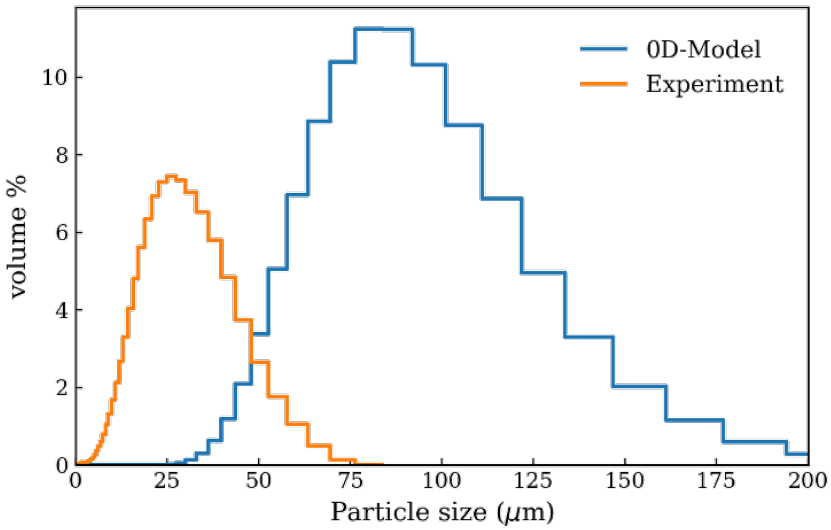

Figure 9: Examples of particle size distributions.

The dynamics of disperse flows is of paramount importance in engineering and offers interesting scientific challenges, due to the complexity of the phenomena involved. Under

some conditions, disperse multiphase systems are monodisperse. Monodisperse implies that all the droplets, bubbles or particles are characterized by the same identical size. Due to the already mentioned phenomena of nucleation, grow, aggregation, agglomeration and breakup, the elements of the disperse phase are characterized a range of size values. This situation is referred to as polydispersity and such a system is defined polydisperse.

The polydispersity is characterized by the droplet, bubble or particle size distribution. Two examples, referring to solid particles dispersed in a fluid, are depicted in Fig. 9, where it is evident that the yellow curve denotes a population of smaller solid particles, whereas the blue curve represents a population or larger and more diverse particles.

From the mathematical point of view the droplet, bubble or particle size distribution, PSD in what follows, is defined so that the following quantity (Marchisio and Fox, 2013; Shiea et al., 2020):

$$n(L)\,\mathrm{d}L$$

represents the number density (i.e. number of particles per unit volume) of particles with size in between L and $L + dL$. A more compact way to represent the PSD is through its moments. The moment of order k of the distribution is defined as follows:

$$m_k = \int_0^\infty n(L) L^k \,\mathrm{d}L. \tag{1}$$

The moment of order zero, m_0, represents the total particle number density, the moment of order one, m_1, represents the total particle length density, the moment of order two, m_2 is related to the specific surface area of the particles, and the moment of order three, m_3, is related to the particle volume fraction. In fact, the specific surface area is: $a = k_a m_2$, whereas the particle volume fraction is: $\alpha_p = k_v m_3$, where k_a and k_v are the area and volume shape factors. For a spherical particle: $k_a = \pi$ and $k_v = \pi/6$, whereas for a cubic particle: $k_a = 6$ and $k_v = 1$. In general for Euclidean objects the ratio between k_a and k_v is equal to six.

The moments of the PSD are also useful to define averaged particle sizes. The number-averaged particle size is defined as the ratio between the moments of order one and zero:

$$d_{10} = \mu = \frac{m_1}{m_0}, \tag{2}$$

the surface-averaged particle size, also known as mean Sauter diameter, MSD, is defined as the ratio between the moments of order three and two:

$$d_{32} = \frac{m_3}{m_2}, \tag{3}$$

whereas the volume-averaged particle size is defined as the ratio between the moments of order four and three:

$$d_{43} = \frac{m_4}{m_3}. \tag{4}$$

For a monodisperse population of particles these different mean particle sizes are all equal and polydispersity is often measured by the distance between these different mean particle sizes. Other measures of polydispersity are the variance of the distribution, defined as follows:

$$\sigma^2 = m_2 - m_1^2, \tag{5}$$

or the coefficient of variation (CoV), defined as follows:

$$CoV = \frac{\sigma}{\mu} = m_0 \sqrt{\frac{m_2}{m_1^2} - 1}. \tag{6}$$

Another quantification of polydispersity is the polydispersity index (PDI) defined via $d_{10\%}$ and $d_{90\%}$. These two numbers can be identified from the cumulative PSD with the following criterion: $d_{10\%}$ is the particle size such that 10 % of the particles are smaller than $d_{10\%}$ and similarly for $d_{90\%}$. PDI can be defined for example as the ratio between $d_{90\%}$ and $d_{10\%}$.

1.6 Relevant dimensionless numbers

Numerous dimensionless numbers are employed to characterize multiphase flows, especially disperse multiphase flows. The most relevant quantities are reported in Tab. 1 and the discussion is here limited to disperse multiphase flows, in which a continuous phase and a disperse phase can be identified. The properties of the disperse phase are identified by the suffix d whereas those of the continuous phase by the suffix c.

The phase-density ratio is simply the ratio between the disperse-phase density and the continuous-phase density; it is useful to identify the importance of inertial effects. The phase-mass ratio is instead the ratio between the disperse-phase mass and the continuous phase mass. When this quantity is small the disperse phase is considered dilute, whereas an increase of this quantity leads to moderately dense and dense systems.

The phase-viscosity ratio is the ratio between the viscosity of the disperse phase and the viscosity of the continuous phase. It is defined only in the case of disperse multiphase systems, with both continuous and disperse phases being fluid. This definition applied therefore only to gas bubbles dispersed in a liquid or liquid droplets dispersed in an immiscible liquid or a gas.

The relative importance of inertial forces (related to the movement of the elements of the disperse phase) and viscous forces (relative to the continuous phase) is represented by the disperse-phase Reynolds number. This number is useful in calculating interfacial forces, such as the drag force, and identifies the type of interaction between the continuous and the disperse phases.

The Eötvöv number measures the importance of gravitational forces compared to surface tension forces and is used (together with Morton number) to characterize the shape of bubbles or drops moving in a surrounding fluid. Figure 10 reports the different observed shapes as a function of the bubble Reynolds number and the Eötvöv number. As it is seen at low values of both dimensionless numbers surface tension forces prevails over gravitational and inertial forces and bubbles are spherical. An increase of both results in the formation of ellipsoidal bubbles, wobbling bubbles, dimpled ellipsoidal-cup, skirted and spherical-cap bubbles.

The Capillary number is a dimensionless quantity representing the relative effect of viscous deformation forces versus surface tension forces acting across an interface between a liquid and a gas, or between two immiscible liquids. For example, an air bubble in a

Table 1: Most relevant dimensionless numbers in disperse multiphase flow. ρ_d and ρ_c are the densities of the disperse and continuous phases, α_d and α_c are the volume fractions of the disperse and continuous phases, μ_d and μ_c are the viscosities of the disperse and continuous phases, $\mathbf{U}_\mathrm{d}$ and $\mathbf{U}_\mathrm{c}$ the velocities of the disperse and continuous phases, d is the diameter of the disperse phase elements, g is the gravity acceleration, σ is the interfacial tension between the disperse and continuous phases, $\dot{\gamma}$ is the shear rate of the continuous phase and τ_c is the characteristic time scale associated with the continuous phase.

Phase-density ratio	$\phi_1 = \rho_\mathrm{d}/\rho_\mathrm{c}$
Phase-mass ratio	$\phi_2 = \rho_\mathrm{d}\alpha_\mathrm{d}/(\rho_\mathrm{c}\alpha_\mathrm{c})$
Phase-viscosity ratio	$\lambda = \frac{\mu_\mathrm{d}}{\mu_\mathrm{c}}$
Disperse-phase Reynolds number	$\mathrm{Re_d} = \frac{\rho_\mathrm{d}\lvert\mathbf{U}_\mathrm{c}-\mathbf{U}_\mathrm{d}\rvert d}{\mu_\mathrm{c}}$
Eötvös number	$\mathrm{Eo} = \frac{d^2 g\lvert\rho_\mathrm{c}-\rho_\mathrm{d}\rvert}{\sigma}$
Morton number	$\mathrm{M} = \frac{g\mu_\mathrm{c}^4\lvert\rho_\mathrm{c}-\rho_\mathrm{d}\rvert}{\rho_c^3\sigma^3}$
Capillary number	$\mathrm{Ca} = \frac{\mu_\mathrm{c}\dot{\gamma}d}{2\sigma}$
Stokes number	$\mathrm{St} = \frac{\rho_\mathrm{d}d^2}{18\mu_c\tau_\mathrm{c}}$

liquid flow tends to be deformed by the friction of the liquid flow due to viscosity effects, but the surface tension forces tend to minimize the surface area.

The Capillary number is often used to established whether or not a bubble or a droplet can breakup, forming daughters, due to the effect of viscous forces, quantified by the shear rate $\dot{\gamma}$. The extent of deformation forces that result in the successful breakup or a bubble or droplet is identified by the critical Capillary number, Ca_{cr}. In the case of pure shear flow the critical Capillary number can be calculated as follows:

$$\log_{10}\mathrm{Ca_{cr}} = -0.506 - 0.0994\log_{10}\lambda + 0.124(\log_{10}\lambda)^2 - \frac{0.115}{\log_{10}\lambda - 0.611}. \tag{7}$$

It is worth mentioning that this expression is valid for $\lambda < 4$, as for $\lambda > 4$ the critical capillary number tends to infinity, implying that for $\lambda > 4$ pure shear flow is not effective in breaking bubbles or droplets. In the case of flows with an elongational component the critical capillary number reads as follows:

$$\mathrm{Ca_{cr}} = 0.14\lambda^{-1/6} \tag{8}$$

Figure 11 reports the dependency of the critical Capillary number versus the phase-viscosity ratio for pure shear flow and pure elongational flow. As it is seen, for every value of the viscosity ratio λ reported, the critical Capillary number for pure elongational flow is smaller than for pure shear flow, indicating that flows with an elongational component are more effective in breaking droplets. This is particularly true for viscous disperse phases, where $\lambda > 4$. In these cases in fact the critical Capillary number for pure shear flows is infinitely large, implying that pure shear flow cannot break the droplet, no matter

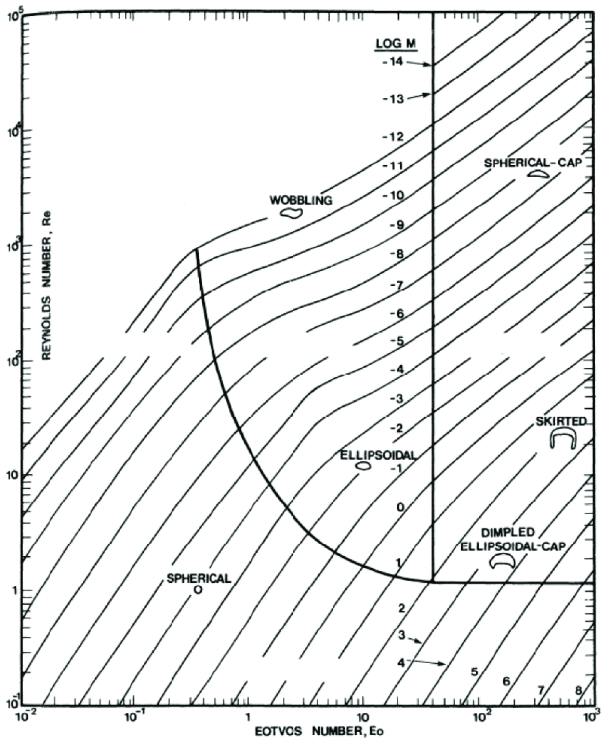

Figure 10: Bubble shapes as a function of the bubble Reynolds number and the Eötvös number. The Morton number is here indicated as M.

how intense is the shear rate. When $\lambda > 4$ only an elongational component can break the droplet.

Eventually it is worth mentioning the Stokes number. This is defined by applying a simple force balance to a bubble, droplet or particle moving within a continuous phase. If only inertia and viscous Stokes drag force is considered, this reads as follows:

$$\rho_{\mathrm{d}} \left(\frac{\pi d^3}{6} \right) \frac{\mathrm{d}\mathbf{v}_{\mathrm{d}}}{\mathrm{d}t} = 3\mu_{\mathrm{c}} \pi d (\mathbf{U}_{\mathrm{c}} - \mathbf{v}_{\mathrm{d}}), \tag{9}$$

where $\mathbf{v}_{\mathrm{d}}$ is the velocity of one single bubble, droplet or particle surrounded by a continuous phase characterized by a velocity equal to $\mathbf{U}_{\mathrm{c}}$. Equation 9 can be rewritten as follows:

$$\left(\frac{\rho_{\mathrm{d}} d^2}{18\mu_{\mathrm{c}}} \right) \frac{\mathrm{d}\mathbf{v}_{\mathrm{d}}}{\mathrm{d}t} = \frac{1}{\tau_{\mathrm{d}}} \frac{\mathrm{d}\mathbf{v}_{\mathrm{d}}}{\mathrm{d}t} = (\mathbf{U}_{\mathrm{c}} - \mathbf{v}_{\mathrm{d}}), \tag{10}$$

where $\tau_{\mathrm{d}} = \frac{\rho_{\mathrm{d}} d^2}{18\mu_{\mathrm{c}}}$ is the characteristic bubble, droplet or particle relaxation time, namely the time required by a disperse phase element to adapt to the local value of the continuous phase velocity $\mathbf{U}_{\mathrm{c}}$. The Stokes number (St) is therefore defined as the ratio between the characteristic time associate with the disperse phase and that associated with the disperse phase. When $\mathrm{St} \ll 1$ the elements of the disperse phase tend to move with the continuous phase, whereas when $\mathrm{St} \geq 1$ the elements of the disperse phase tend to have their own independent velocity. Under these conditions interesting phenomena, such as Particle Trajectory Crossing (PTC), occur.

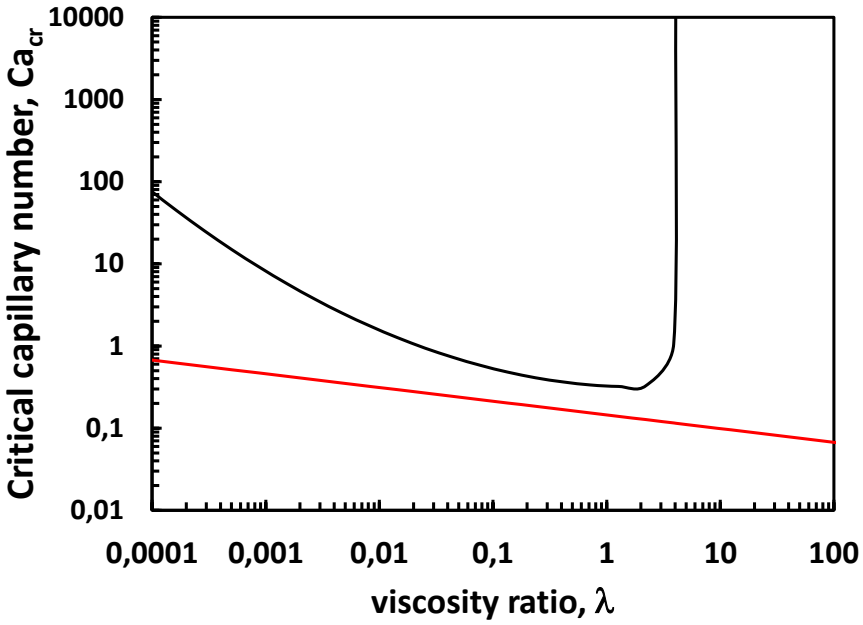

Figure 11: Dependency of the critical Capillary number, Ca_{cr} versus the viscosity ratio for pure shear flow (black line) and pure elongational flow (red lines).

1.7 Phase coupling

Figure 12 sketches the different regimes of interactions between the continuous and disperse phases. Under the one-way coupling regime the continuous phase affects the trajectory and velocity of the elements of the disperse phase, however the disperse phase is so diluted that the continuous phase is not affected by the presence of the disperse phase. Viceversa, when the phase-mass ratio increases the continuous phase affects the evolution of the disperse phase and the disperse phase affects the motion of the continuous phase. A further increase in the phase-mass ratio leads to interactions between the elements of the disperse phase, due to their proximity, via their wakes. This interaction intermediated by the continuous phase is called three-way coupling. Finally when the elements of the disperse phase are very dense they interact directly, resulting in collisions, that can in turn lead to coalescence, aggregation or agglomeration.

1.8 Discrete phase element evolution

In many multiphase flows the disperse phase evolves not only because of momentum transfer with the continuous phase but also because of phenomena that lead to the formation of new elements of the disperse phase (i.e. nucleation) and to their continuous transformation due to molecular growth, aggregation, agglomeration, breakage and deposition. They are usually classified depending on their order.

Zero-order processes are those in which the evolution of the disperse phase do not depend on the disperse phase, but on the continuous phase only. Among them the most important is primary homogeneous nucleation, in which new elements of the disperse phase are formed by some physical and chemical phenomena occurring in the continuous phase. Relevant examples are condensation of droplets in the gas phase, formation of droplets of an immiscible liquid in the bulk of another liquid, due to a temperature reduction, or formation of a solid phase (i.e. solid particles) due to a chemical reaction occurring in the continuous phase or a temperature reduction which decreases the solubility of a solute.

Once the elements of the disperse phase are formed they can growth and shrink due to addition or depletion of single molecules. This is called molecular growth and is typically described as a continuous process. Relevant examples are the growth of droplets suspended in a supersaturated gas, the evaporation of droplets in an undersaturated gas phase, or the growth or dissolution of solid particles in a liquid.

First-order processes are those whose rate is proportional to the concentration of disperse phase elements. The most common example is breakage or breakup. Droplets or bubbles suspended in a liquid or a gas can break because of deformation and shear on the continuous phase. Relevant engineering examples are droplets of a spray and bubbles or solid particles in liquid. The rate with which droplets, bubbles or particles breakup is usually written with a first-order kinetics, namely the rate is proportional to their concentration in the continuous phase and the proportionality constant is called breakup kernel. Another engineering example is droplet or particle deposition on the walls of duct or vessel or on the walls of a porous medium, as in the case of filtration.

Second-order processes are instead those whose rate is proportional to the concentration of the disperse phase elements to the second power. In this category we find aggregation, agglomeration and coalescence. The term aggregation is usually employed in

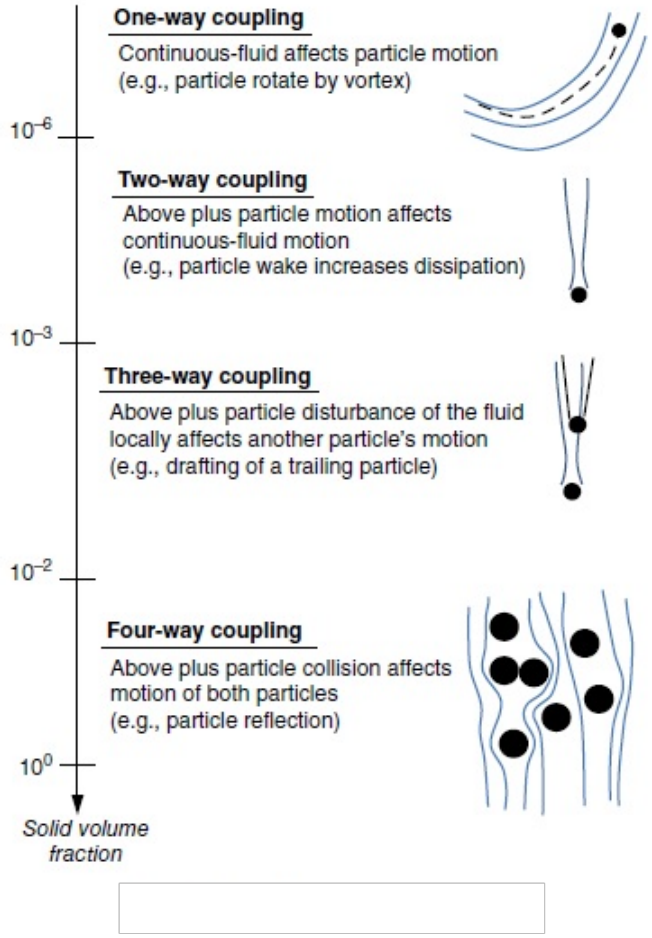

Figure 12: Sketch representing the different regimes of interactions between the continuous and disperse phases, labelled as one-, two-, three- and four-way coupling.

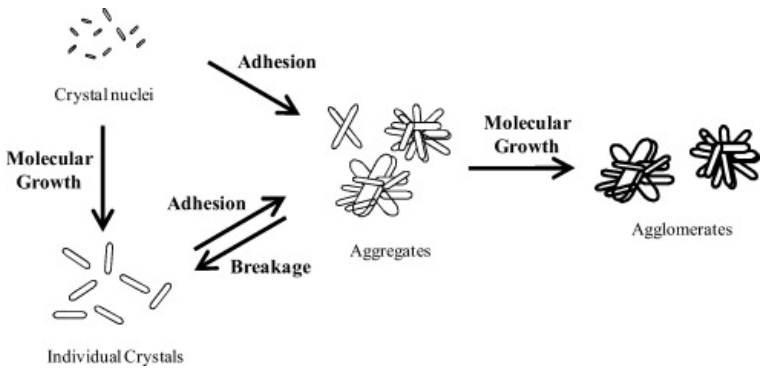

Figure 13: Sketch representing the difference between aggregation and agglomeration.

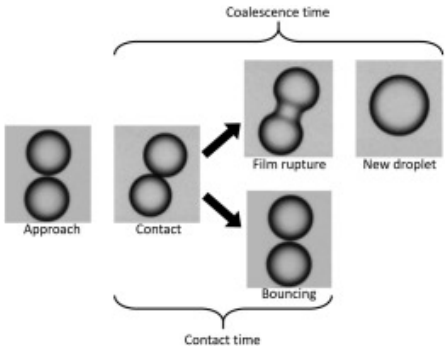

Figure 14: Sketch representing the main steps involved during coalescence.

the context of solid particles sticking together because of secondary-forces, such as attractive Van der Waals interactions. Aggregation is typically reversible and aggregates, due to the flow of the continuous phase, can easily breakup into the original primary particles. Agglomeration, also used in the context of solid particles, is instead typically considered irreversible. During agglomeration, particles after colliding and sticking together form stable chemical bonds (e.g. thanks to molecular growth), which are difficult to break because of flow deformation and shear in the continuous phase. Figure 13 sketches the main difference between aggregation and agglomeration. The term coalescence is employed in the context of liquid droplets or gas bubbles. Droplets and bubbles to coalesce need to collide and interact together for a time interval, long enough to allow the drainage of the continuous phase entrapped between them. In these cases not only the viscous resistance of the draining film is important, also the attractive forces between the two approaching interfaces play an important role. The involved steps are schematically represented in Fig. 14.

2 Classification of computational models

A plethora of methods is available for the simulation of multiphase flows. They are generally classified depending on a number of criteria and they are summarized in Fig. 15. As evident from the figure the computational models are characterized by an increase of accuracy and computational costs when moving from left to right.

2.1 Molecular dynamics models

A first classification is based on the type of approach employed to describe the multiphase systems. When the molecules appearing in the involved phases are explicitly described the computational model is often labelled as atomistic. Among atomistic models different options are available, namely: full-atom molecular dynamics (FAMD), dissipative particle dynamics (DPD), smoothed particle hydrodynamics (SPH) and Lattice Boltzmann method (LBM). All these are particle-based meshless models in which the particles representing atoms, molecules or groups of molecules, are free to move in the computational domain which is not discretized by using for example the finite-difference (FD), the finite-element (FE) or the finite-volume (FV) schemes.

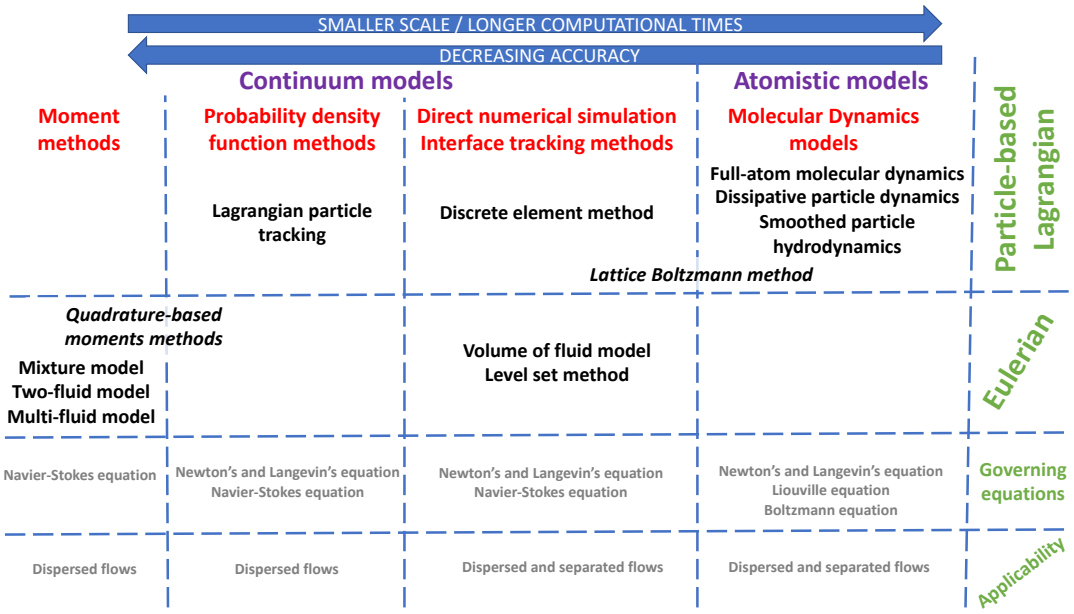

Figure 15: Possible classification of computational models for multiphase flows.

In FAMD all the atoms composing the involved molecules are explicitly tracked and interact with each other via bonded and non-bonded interactions. Bonded interactions represent chemical bonds between atoms and are represented by using different types of potentials (e.g. Harmonic potential) whereas non-bonded interactions represent attractive and repulsive forces exchanged between atoms belonging to different molecules. They are typically represented by the Lennard-Jones potential. The values for the parameters appearing in these potentials are tabulated in force fields, such as for example AMBER, CHARMM, GROMOS and OPLS, just to cite a few (Bazzano et al., 2019; Lavino et al., 2018; Karimi et al., 2018; Lavino et al., 2017; Di Pasquale et al., 2014).

The main limit of FAMD stands in the length- and time-scales explorable and therefore the computational model is often coarse-grained to integrate out the faster degrees of freedom. One very popular approach is the so-called MARTINI force field (Lavino et al., 2020). In some cases not only atoms are grouped together forming super-atoms or beads, but also molecules are groups together in beads. One such approach is dissipative particle dynamics (DPD) where the number of molecules coarse-grained in one bead is the so-called coarse-graining factor, N_{m} (Boccardo et al., 2019a; Pasquino et al., 2019; Droghetti et al., 2018). Since the beads in DPD now represent groups of molecules they can interpenetrate each other resulting in the use of soft-potentials, on the contrary of what happens in FAMD. Moreover, the coarse-grained degrees of freedom must be accounted for and this is typically done by including not only conservative forces (such as the bonded and non-bonded interactions described above) but also considering dissipative and stochastic forces. These two contributions must be balanced and this is usually done by making use of the fluctuation dissipation theorem. An approach similar to DPD is the smoothed particle hydrodynamics (SPH) and the Lattice Boltzmann methods (LBM). The LBM is reported in Fig. 15 in between atomistic and continuum models as it is often interpreted as a continuum model.

Another interesting point is the governing equations involved. In the case of FAMD the governing equations, written in terms of the trajectories of the single atoms involved, are the Newton equation of motion. In the case of DPD instead the introduction of the dissipative and stochastic terms transform the Newton equation in the so-called Langevin's equation. When the same models are instead written in terms of the corresponding distribution functions in this case the main governing equation is the Liouville equation, whose equilibrium solution is the Maxwell-Boltzmann distribution. In the case of the LBM the main governing equation is instead the Boltzmann equation. Atomistic models are usually solved in a Lagrangian framework, namely by tracking the evolution of each individual trajectory of the particles representing atoms, in the case of FAMD, or groups or atoms and molecules, in the case of DPD, SPH or LBM. These methods can be indifferently applied to the description of separated multiphase flows, as well as disperse multiphase flows.

2.2 Direct numerical simulation

When the continuum hypothesis holds the atomistic description of the multiphase flow can be discarded and the involved phases can be described as continuous phases. In this case the model is generally labelled as direct numerical simulation (DNS) or interface tracking method (ITM). In the case of fluid-fluid multiphase systems, namely gas-liquid or liquid-liquid flows, the most popular methods are the volume-of-fluid (VOF) model and the level-set method (LSM). In both approaches the presence of one phase or another is indicated by an indicator or color function which assumes for example values equal to one when one phase is present and zero when the other one is present. VOF and LSM differ on the way in which the interface is directly tracked. The governing equations are in this context usually solved in an Eulerian framework as briefly described in the following sections. It is interesting to notice here that the continuum hypothesis holds as long as the involved phases can be described as continuous. When for example two bubbles suspended in the liquid merge and coalesce, or when two droplets dispersed in a

gas or a liquid merge and coalesce, the rupture of the film undergoing drainage cannot be treated by continuum models. This is caused by the emergence of molecular forces (e.g. van der Waals intermolecular forces) that require the use of surrogate models to describe coalescence or bubbles and droplets with VOF and LSM. In the case of solid-gas or solid-liquid systems, solid particles are described within the Lagrangian framework, resulting in the so-called discrete element method (DEM) usually coupled with an Eulerian solver to describe the evolution of the continuous phase (Frungieri et al., 2020). Also in the DEM the interface between the solid particles and the surrounding gas or liquid is tracked explicitly, as long as the continuum hypothesis holds. This is not valid for example during particle-particle collisions, when a small amount of continuous phase is entrapped within the two colliding particles. Also in this case to account for the effect of molecular forces surrogate models are necessary. A relevant example in this context is that of lubrication forces, particular important in solid-liquid systems, otherwise negligible in solid-gas systems. VOF and LSM can indifferently applied to separated and dispersed multiphase flows. DEM is instead applied to describe solid-gas and solid-liquid systems, which are inherently dispersed.

2.3 Probability density function methods

The explicit tracking of the interface characterizing VOF, LSM and DEM results in great accuracy, which allows to reduce the number of simplification hypothesis and simplifications, expect for the continuum hypothesis, and large computational costs. To reduce the associated computational costs a possibility is to neglect the details of the evolution of the interface(s) present and focus instead on the probability density function (PDF) characterizing the state of the multiphase system. This PDF can be written for example in terms of the velocity of the bubbles, droplets or solid particles involved, and in terms of other relevant properties, such as for example temperature, concentration of species, size and/or shape. In this case the governing equation is a kinetic equation that dictates the evolution of the PDF characterizing the elements of the disperse phase. This governing equation is often called Boltzmann equation, when the internal variables (or internal coordinates) are the velocities (or momenta) of the elements of the disperse phase. The term generalized population balance equation (GPBE) is instead employed when the internal variables or coordinates are both velocities and mass, volume or size of the disperse phase elements. These PDF methods can theoretically be solved by using both Eulerian and Lagrangian approaches. Eulerian methods require the discretization of the internal coordinates by using for example the same numerical methods employed to discretize space and time. However, the dimensionality of the problem (i.e. one time variable, three spatial coordinates, three velocity coordinates, ...) leads to very high computational costs. For this reason these computational models are often solved in a Lagrangian framework, by using individual particle tracking, and by following the evolution over time of one possible realization or of multiple realizations. Thanks to the Ergodic theorem averaged properties are estimated by using time-, space- and/or ensemble averages. For these methods the governing equations are the Navier-Stokes equation for the continuous phase and the Newton or Langevin equations for the disperse phase. They are typically applied to disperse multiphase systems.

2.4 Moment methods

With these PDF methods larger systems can be simulated but some limitations are present. In particular, dense systems, when the number of disperse phase elements is very large, are intractable, unless the concept of notional particle is employed. Moreover some additional limitation in the grid size needs to be addressed. To overcome these limitations the model can be written in terms of the moments of the PDF of the involved variables. These methods are called moment methods (MoM). One of the most popular version is the so-called two-fluid model (TFM). In the TFM balance equations for the relevant properties (e.g. volume fractions and momentum) are written and solved for two phases: the continuous and the disperse phases. The TFM was formulated for disperse two-phase flows but can be applied, to a certain extent, also to separated flows (generally neglecting interfacial forces). In its basic formulation the TFM is constituted by a continuity equation for the disperse phase, which dictates the evolution of the volume fraction of the disperse phase, a two momentum balance equations for both the continuous and disperse phases. The governing equations for the TFM are very similar to the continuity equation and the Navier-Stokes equations for single-phase systems, solved for both the involved phases.

The extension to multiphase systems with more than two phases, is the so-called multi-fluid model (MFM). In the MFM transport equations for volume fractions and phase velocities are solved similarly to what described for the TFM. The MFM is often also used to simulate two-phase systems characterized by large polydispersity. Let us imagine for example a gas-liquid systems with very small bubbles suspended in a liquid together with large bubbles. Clearly the small bubbles will behave very differently from large bubbles and therefore one option is to consider the system as constituted by three phases: the continuous primary liquid phase, plus two disperse secondary bubbly phases, one representing the small bubbles and one representing the large bubbles.

Under some conditions, typically when the Stokes number is moderately large, solving a momentum balance equation for the disperse phase(s) might be unnecessary, as the elements of the disperse phase almost instantaneously adapt to the local flow field imposed by the continuous phase. In this case one single momentum balance equation is written for the multiphase mixture, constituted by the continuous phase and the additional disperse phase(s). For this reason this approach is known as the mixture model (MiM). The velocity of the single phases can then be retrieved by using the instantaneous equilibrium hypothesis, solving an algebraic equation, rather than a differential transport/balance equation. Different strategies are adopted to do this and one of the most popular is the algebraic slip model (ASM).

The MiM, TFM and MFM are often coupled with a population balance equation (PBE) to describe the evolution of the size distribution of the elements of the disperse phase, described in Section 1.5 at pag. 10. In the context of MoM one very popular approach is the quadrature method of moments QMOM in which the PBE is written in terms of the moments of the PSD as introduced in Eq. (1). Several variations of this method have been proposed in the literature and they are generally known as quadrature-based moment methods (QBMM). One popular open-source implementation is called openQBMM (Passalacqua et al., 2018). These methods are summarized in Table 2 and readers interested in more details are referred to the book of Marchisio and Fox (2013).

An alternative but more expensive approach is the method of classes that in one popular implementation for multiphase flows is called the MuSiG model.

2.5 Interfacial forces

In the case of molecular dynamics models and direct numerical simulations no assumptions need to be made on the exchange of momentum, realized by interfacial forces, as they are directly evaluated by the models themselves. In the case of PDF methods and MoM instead specific models for the interfacial forces need to be formulated and employed. In what follows the most important are discussed.

Drag force. Among the many relevant interaction forces that must be accounted for in disperse multiphase systems, the most important is drag force. In the case of an isolated bubble/droplet/particle the following expression can be used:

$$\mathbf{F}_{\mathrm{D}} = C_{\mathrm{D}} A_{\mathrm{D}} \frac{1}{2} \rho_{\mathrm{c}} |\mathbf{U}_{\mathrm{c}} - \mathbf{U}_{\mathrm{d}}| \left(\mathbf{U}_{\mathrm{c}} - \mathbf{U}_{\mathrm{d}}\right), \tag{11}$$

where A_{D} is the bubble/droplet/particle cross section area and C_{D} is the drag coefficient. If the force is divide by the mass of the bubble/droplet/particle the acceleration can written as follows:

$$\mathbf{A}_{\mathrm{D}} = \frac{C_{\mathrm{D}} A_{\mathrm{D}}}{2 V_{\mathrm{d}}} \frac{\rho_{\mathrm{c}}}{\rho_{\mathrm{d}}} |\mathbf{U}_{\mathrm{c}} - \mathbf{U}_{\mathrm{d}}| (\mathbf{U}_{\mathrm{c}} - \mathbf{U}_{\mathrm{d}}) \tag{12}$$

where $A_{\mathrm{D}}/V_{\mathrm{p}}$ is the ratio between cross section area and volume equal to $3/(2d)$ for spheres. As already mentioned ρ_{c} is the density of the continuous phase, ρ_{d} is the density of the disperse phase, d is the diameter of the bubble/droplet/particle and $\mathbf{U}_{\mathrm{c}}$ and $\mathbf{U}_{\mathrm{d}}$ are the characteristic velocities of the continuous and disperse phase, respectively.

In the case of solid particles and creeping (or Stokes) flow, the following definition for the drag coefficient can be used:

$$C_{\mathrm{D}} = \frac{24 \nu_{\mathrm{c}}}{|\mathbf{U}_{\mathrm{c}} - \mathbf{U}_{\mathrm{d}}| d} = \frac{24}{\mathrm{Re}_{\mathrm{d}}}, \tag{13}$$

Table 2: Classification of QBMM. QMOM can be used only when 1 internal coordinate (e.g. particle size) is used and is based on a discrete reconstruction of the PSD. The direct QMOM can handle more than one internal coordinate as well as, the conditional QMOM. DQMOM always guarantees moment realizability. The extended QMOM is based on a continuous reconstruction of the PSD.

Name	PSD reconstruction	N. int. coordinates	Moment realizability
QMOM	Discontinuous	1	with appropriate schemes
DQMOM	Discontinuous	>1	always guaranteed
CQMOM	Discontinuous	>1	with appropriate schemes
EQMOM	Continuous	1	with appropriate schemes

where $\nu c = \frac{\mu_c}{\rho_c}$ is the kinematic viscosity of the continuous phase and $\mathrm{Re_d}$ is the bubble/droplet/particle Reynolds number. The expression in Eq. (13) is of course valid only for a sphere characterized by very small slip velocity[1], and is generally assumed valid for $\mathrm{Re_d} \leq 0.1$. For spherical particles at higher particle Reynolds numbers, the following corrections can be used:

$$C_\mathrm{D} = \begin{cases} \left[\left(\frac{24}{\mathrm{Re_d}}\right)^{1/2} + 0.5407\right]^2 & \text{for } 0.1 < \mathrm{Re_d} < 6000, \\ 0.445 & \text{for } 6000 < \mathrm{Re_d} < 10^5. \end{cases} \tag{14}$$

These equations are valid for isolated spherical particles when the surrounding continuous phase can be treated as a continuum (as opposed to a rarefied gas). To establish whether or not the continuum hypothesis is valid the ratio between the mean free path for the continuous phase (i.e., average time interval between two subsequent collisions of the molecules constituting the primary phase) to the particle size is generally employed:

$$\mathrm{Kn} = \frac{\lambda_\mathrm{f}}{d}. \tag{15}$$

When this quantity is much smaller than unity, the continuum approach for describing the interactions between the primary phase and the elements of the secondary phase is appropriate. When this ratio is bigger than unity, the interactions between the primary phase and the elements of the secondary phase must be described in terms of individual molecules impacting and rebounding onto the particle surface; this is the so-called free-molecular regime. For intermediate values the interactions between the primary and secondary phases are in the slip regime, where the continuum approach for the primary phase can still be used with some corrections, to account for the velocity jump between the fluid adjacent to the surface of the particle. This correction results in the following expression for the drag coefficient:

$$\frac{C_\mathrm{D}^*}{C_\mathrm{D}} = \frac{1}{1 + \mathrm{Kn}\left[2.49 + 0.84\exp\left(-\frac{1.74}{\mathrm{Kn}}\right)\right]}, \tag{16}$$

which is commonly referred to as the Cunningham correction factor.

The calculation of the drag coefficient, C_D, in gas-liquid and liquid-liquid systems, when the elements of the disperse phase are bubbles or droplets, is complicated by impurities present in the continuous phase and by the fact that bubbles and droplets can change their shapes. For clean systems (i.e. no impurities) the following expression is obtained:

$$C_\mathrm{D} = \max\left\{\min\left[\frac{16}{\mathrm{Re_d}}(1 + 0.15\mathrm{Re_d^{0.687}}), \frac{48}{\mathrm{Re_d}}\right], \frac{8}{3}\left(\frac{\mathrm{Eo}}{\mathrm{Eo}+4}\right)\right\}. \tag{17}$$

The correlation used for slightly contaminated systems is:

$$C_\mathrm{D} = \max\left\{\min\left[\frac{24}{\mathrm{Re_d}}(1 + 0.15\mathrm{Re_d^{0.687}}), \frac{72}{\mathrm{Re_d}}\right], \frac{8}{3}\left(\frac{\mathrm{Eo}}{\mathrm{Eo}+4}\right)\right\}, \tag{18}$$

[1]The slip velocity is defined as the different between the continuous and disperse phase velocities: $\mathbf{U_s} = \mathbf{U_c} - \mathbf{U_d}$.

whereas for fully contaminated systems the following correlation is employed:

$$C_{\mathrm{D}} = \max\left[\frac{24}{\mathrm{Re_d}}(1+0.15\mathrm{Re_d^{0.687}}), \frac{8}{3}\left(\frac{\mathrm{Eo}}{\mathrm{Eo}+4}\right)\right]. \tag{19}$$

Impurities accumulating the bubble or droplet interface are important as they affect the mobility of the interface. When no impurities are present the interface is fully mobile and the drag force is smaller than that of a solid particle with the same volume and size. For slightly and fully contaminated systems the interface between the bubble/droplet and the continuous phase sees an accumulation of impurities that make the interface immobile, resulting in larger drag forces.

These relationships are valid for isolated bubbles or droplets moving under laminar flow conditions. In the case of turbulent flow, the effect of turbulent eddies impinging on the bubble surface is to increase the drag force. This is typically accounted for by introducing an effective viscosity (rather than the molecular viscosity of the continuous phase, μ_{c}) defined as:

$$\mu_{\mathrm{c,eff}} = \mu_{\mathrm{c}} + C_{\mathrm{l}}\rho_{\mathrm{c}}\varepsilon_{\mathrm{c}}^{1/3}d^{4/3}$$

, where ε_{c} is the turbulent dissipation rate in the fluid phase and C_{l} is a constant usually taken equal to 0.02. This effective viscosity, used for the calculation of the bubble/particle Reynolds number, accounts for the turbulent reduction of slip due to the increased momentum transport around the bubble, which is in turn related to the ratio of bubble/doplet size and turbulent length scale.

Another correction often employed is the one accounting for three-way coupling. As explained when the disperse phase becomes dense bubbles/droplets/particles interact with each other through their wakes. The concentration of the disperse phase elements is quantified by the disperse phase volume fraction, α_{d}, which for a two-phase system is related to the continuous phase volume fraction by the following expression: $\alpha_{\mathrm{c}} = -\alpha_{\mathrm{c}}$. In the case of solid particles one of the most popular correlations to account for these effects is the following:

$$C_{\mathrm{D}} = \frac{24}{\mathrm{Re_d}}\left[1+0.15(\alpha_{\mathrm{c}}\mathrm{Re_d})^{0.687}\right]\alpha_{\mathrm{c}}^{-\beta}. \tag{20}$$

where $\beta = 3.65$ is a correction factor to account for the presence of other particles. In this case, when the particulate system is very dilute (i.e., $\alpha_{\mathrm{c}} \approx 1$), Eq. (20) reduces to a simpler expression.

Lift force. Particles moving in a fluid with mean shear experience a lift force perpendicular to the direction of fluid flow. The shear lift originates from inertia effects in the viscous flow around the particle and depends on the mean vorticity of the fluid phase. For a spherical particle, the particle acceleration due to the lift force (also known as the Saffman lift force) is equal to:

$$\mathbf{A}_{\mathrm{L}} = C_{\mathrm{L}}\frac{\rho_{\mathrm{f}}}{\rho_{\mathrm{p}}}(\mathbf{U}_{\mathrm{c}} - \mathbf{U}_{\mathrm{d}}) \times (\nabla \times \mathbf{U}_{\mathrm{c}}) \tag{21}$$

where C_{L} is the lift coefficient that can be derived from the theory. Conflicting conclusions concerning the importance and the significance of the lift force can be found in the

literature. For example, some authors reported that the lift force seems to be necessary for the accurate representation of flow behavior in gas-liquid systems and the work of Monahan et al. (2005) demonstrated the importance of the lift force to the stability of homogeneous flow predictions when using the TFM. Other authors showed that C_{L} should be taken equal to 0.5 to ensure good agreement with experiments. The same value has been reported elsewhere whereas Drew and Passman (1999) suggest using $C_{\mathrm{L}} = 0.25$. Other authors determined an empirical correlation for the net transverse lift coefficient valid for gas-liquid systems. For air bubbles suspended in water for $d < 4.4$ mm, C_{L} was found to be a function of Re_{p}, whereas for $d_{\mathrm{p}} > 4.4$ mm, C_{L} was found to be a function of the Eötvös number. Also, the sign of C_{L} changed from positive to negative when $d = 5.8$ mm. Other similar correlations based on the capillary number have been proposed (Sankaranarayanan and Sundaresan, 2002), showing that for the majority of the applications C_{L} should be positive.

2.6 What about turbulence?

In many industrial applications involving multiphase flows the flow regime is turbulent and different strategies are generally employed to deal with this problem. One option is to resolve all the involved length- and time-scales with no simplification assumption. This is called direct numerical simulation (DNS) and is extremely expensive from the computational point of view. An interesting alternative is to filter out some of smaller scales, which can be modeled, by using for example the Kolmogorov theory, and directly simulate the larger ones. The model employed to describe the dissipation of turbulent kinetic energy at the smallest scales is often referred to as sub-grid scale model. This second approach is called large eddy simulation (LES) and is very popular in industrial applications. One last approach is based on the Reynolds-average theory. A fluctuating turbulent property can be time-averaged; time-averaging is, thanks to the Ergodic theorem, equivalent to ensemble-averaging. The governing equations, after time-average, also known in this context as Reynolds-average, present some unclosed terms that need to be modeled. The most popular closure models are based on the isotropy hypothesis and assume that momentum transfer due to turbulent fluctuations and eddies is proportional to the average velocity gradient, by using the so-called Bousinnesq approximation. This latter approach is known as Reynolds-averaged Navier-Stokes equation (RANS) approach and is often formulated in terms of the continuous phase kinetic energy, k_{c}, and the continuous phase turbulence dissipation rate, ε_{c}.

2.7 Guidelines for choosing a model

Since numerous models are available for the simulation of multiphase flows it is extremely important to develop guidelines that help modelers to choose the best one for their specific needs and computational resources available. Different criteria can be followed and Fig. 16 reports one of them. When the size of the particles, d, is extremely small with respect to the Kolmogorov length-scale[2] associated with the continuous phase, η, the so-called dust gas model can be used. In this model it is assumed that all the bubbles/droplets/particles

[2]The Kolmogorov microscales are the smallest scales in turbulent flow. At the Kolmogorov scale, viscosity dominates and the turbulent kinetic energy is dissipated into heat. The Kolmogorov length-

move with the continuous phase and their velocity is identical to that of the continuous phase. This is a particular case of the MiM and is indicated in Fig. 16 as dusty gas model. As the ratio $\frac{d}{\eta}$ increases more complex approaches should be used, as for example the MiM together with the ASM (indicated as equilibrium Eulerian in Fig. 16) or the TFM or MFM indicated in Fig. 16 as Eulerian. When the particle-to-Kolmogorov scale ratio reaches unity PDF methods must be used and eventually when the ration is much grater than unity DNS should be employed.

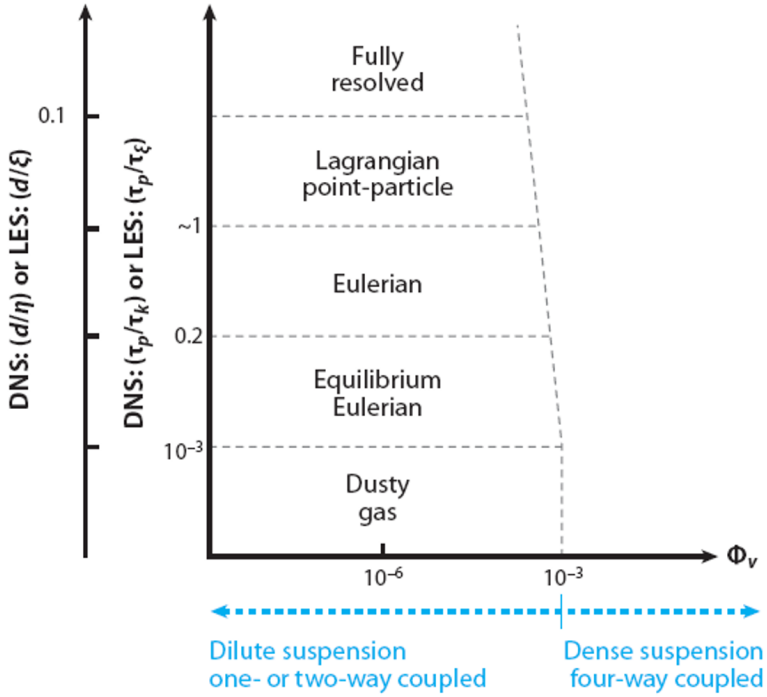

Figure 16: Guidelines for choosing a multiphase flow model among direct numerical simulation (fully resolved), PDF methods (Lagrangian-point particles), and MoM (Eulerian, Equilibrium Eulerian and dusty gas model). The y-axis of the plot reports the ratio between the bubble/droplet/particle size and the Kolmogorov length-scale associated with the continuous phase. The x-axis reports the volume fraction of the disperse phase.

Another interesting criterion is in terms of the Stokes number, summarized in Fig. 17. When the Stokes number is very small, the elements of the disperse phase tend to move with the continuous phase and the dusty gas model can be used. As the Stokes number increases the MiM coupled with the ASG or the TFM should be used instead.

A third parameter that should be considered when selecting a computational model for a multiphase system is the polydispersity index (PDI). When the PDI is small all the bubble/droplets/particles can be considered as monodisperse and their velocity can be calculated by any of the above mentioned methods by using a mean particle size. As PDI

scale is defined as follows: $\eta = \left(\frac{\nu_c^3}{\varepsilon_c}\right)^{1/4}$, where ε_c is the average rate of dissipation of turbulence kinetic energy per unit mass for the continuous phase and ν_c is the kinematic viscosity of the continuous phase.

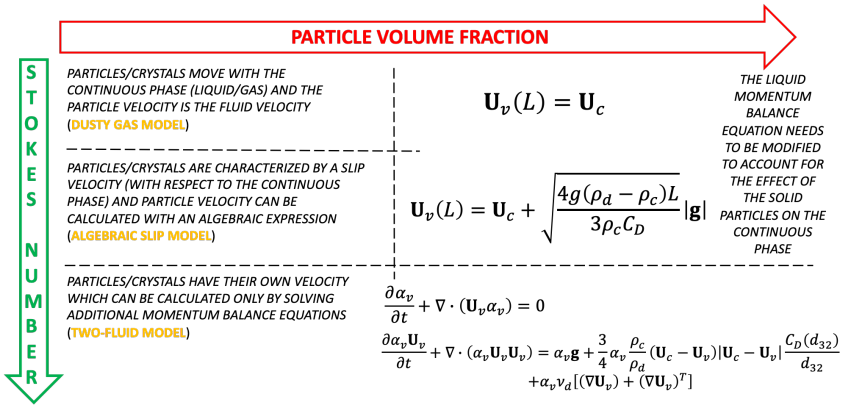

Figure 17: Guidelines for selecting a multiphase model based on the concentration of the disperse phase (particle volume fraction) and the Stokes number.

increases the population of bubbles/droplets/particles must be represented by multiple size values, resulting for example in the use of the MFM.

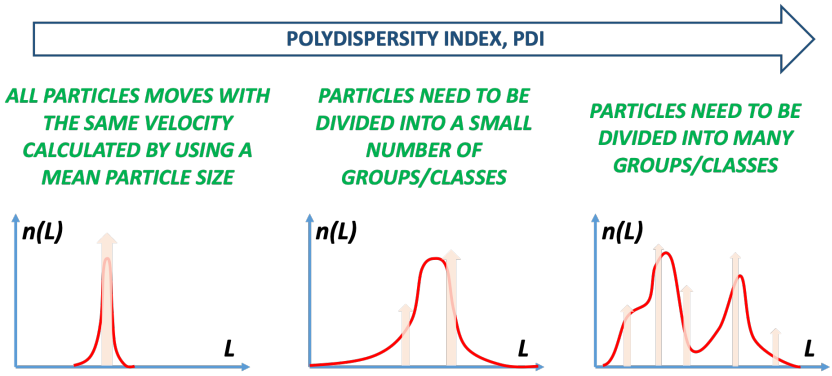

Figure 18: Guidelines for selecting a multiphase model depending on the polydispersity index (PDI).

In summary there are three parameters that can be used to identify the best computational model for a multiphase flow: bubble/droplet/particle concentration, Stokes number and polydispersity. When the phase-mass ratio, defined by: $\phi_2 = \rho_\mathrm{d}\alpha_\mathrm{d}/(\rho_\mathrm{c}\alpha_\mathrm{c})$, is much smaller than one the system can be considered dilute with one-way momentum coupling, whereas when $\rho_\mathrm{d}\alpha_\mathrm{d}/(\rho_\mathrm{c}\alpha_\mathrm{c}) \geq 0.1$ two-way momentum coupling is required. We consider the small particle Stokes number limit to be identified by $\mathrm{St} \ll 1$, whereas moderate and large Stokes numbers are identified by $\mathrm{St} \approx 1$ and $\mathrm{St} \geq 1$, respectively. It is important to keep in mind that in general the Stokes number can vary from physical point to physical point in the system, depending on the definition of the characteristic time-scale for the continuous phase. Polydispersity can instead be identified by a polydispersity index (PDI), defined as the ratio between the size of the largest/heaviest particles and the smallest/lightest particles.

Based on the expected polydispersity of the multiphase systems and the type of processes that the multiphase system undergoes, the corresponding bubble/droplet/particle velocity can be calculated using one of the following continuum models:

1. **Pseudo-homogeneous or dusty-gas model:** very small particle Stokes number and limited polydispersity (momentum balance equation only for the continuous phase if the system is dilute or for the mixture of continuous and disperse phases if the system is dense).

2. **Mixture model (MiM) and algebraic slip velocity model (ASM) with a single velocity based on the mean particle size:** small particle Stokes number and limited polydispersity (momentum balance equation only for the continuous phase if the system is dilute or for the mixture of continuous and disperse phases if the system is dense).

3. **Mixture model (MiM) and algebraic slip velocity model (ASM) with multiple disperse phase velocities:** small particle Stokes number and non-negligible polydispersity (momentum balance equation only for the continuous phase if the system is dilute or for the mixture of continuous and disperse phases if the system is dense).

4. **Two-fluid model (TFM) with a single velocity based on the mean particle size:** moderate particle Stokes number and limited polydispersity (in both dilute and dense systems).

5. **Multi-fluid model (MFM) with multiple disperse phase velocities:** moderate particle Stokes number and large polydispersity (in both dilute and dense systems).

3 Computational models for multiphase flows

In this section we focus on some of the computational models introduced in the previous sections. With a focus on volume-of-fluid (VOF) model, level set method (LSM), two-fluid model (TFM), multi-fluid model (MFM) and mixture model (MiM).

3.1 General governing equations

All the above-mentioned continuum models are derived starting from the continuity and Navier-Stokes equations. Given $\rho(\mathbf{x}, t)$ and $\mathbf{U}(\mathbf{x}, t)$, the density and velocity of a fluid at time t and position $\mathbf{x}$, the continuity equation can be written as follow:

$$\frac{\partial \rho}{\partial t} + \nabla \cdot (\rho \mathbf{U}) = 0, \tag{22}$$

whereas the momentum balance equation, which becomes the Navier-Stokes equation for an incompressible Newtonian fluid, reads as follows:

$$\rho \left(\frac{\partial \mathbf{U}}{\partial t} + \mathbf{U} \cdot \nabla \mathbf{U} \right) = \nabla p - \mu \nabla^2 \mathbf{U} + \rho \mathbf{g}, \tag{23}$$

where ρ is the density of the fluid and μ is its viscosity. These equations are further modified and transformed to derive the governing equations of VOF, LSM, TFM, MFM and MiM. A more detailed discussion can be found in the cited literature and in the work of Tronci (2021).

3.2 Level Set Method

The LSM was developed for the first time by Osher and Sethian (1988) and consists in the transport by the fluid velocity of the signed distance ϕ, that is called *level set function*:

$$\frac{\partial \phi}{\partial t} + \mathbf{U} \cdot \nabla \phi = 0. \tag{24}$$

As mentioned this is usually employed to simulate fluid-fluid multiphase systems, such as gas-liquid or liquid-liquid systems and flows. This is the Eulerian formulation of the level set equation, in which the interface is *captured* by ϕ. An alternative is the use of a Lagrangian approach, which however suffers from a number of drawbacks, as for example the one described in Fig. 19 Osher et al. (2002).

In what follows the discussion is limited to the Eulerian approach for the LSM and to two-phase systems. For a two-phase systems the level set function, ϕ, is generally defined to be zero the interface, while the negative values of ϕ defines the region occupied by one phase and positive values the region occupied by the other phase:

$$\phi(\mathbf{x}, t) \begin{cases} > 0 & \text{if } \mathbf{x} \in \text{phase 1} \\ = 0 & \text{if } \mathbf{x} \in \partial\Omega \\ < 0 & \text{if } \mathbf{x} \in \text{phase 2} \end{cases} \tag{25}$$

In the LSM the versor normal to the interface and the curvature of the interface are easily defined respectively as:

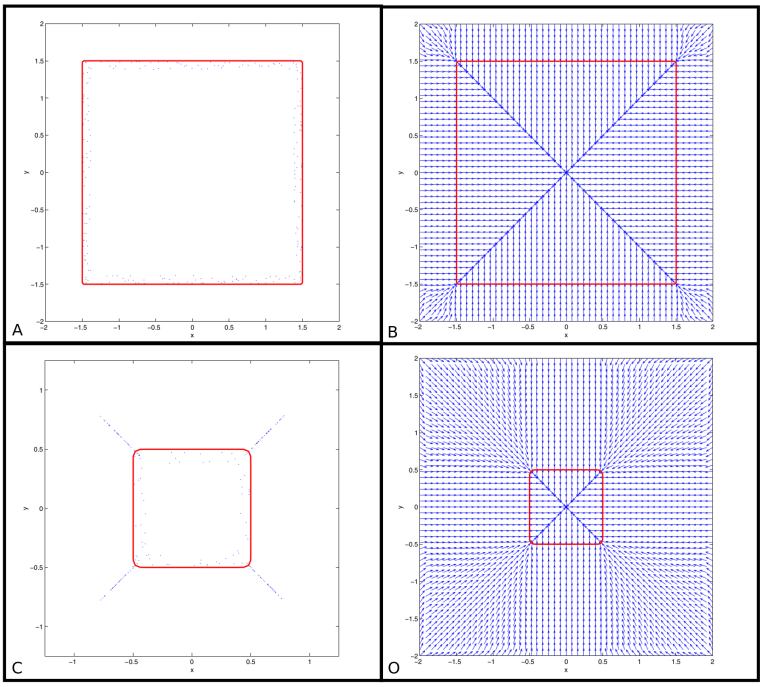

Figure 19: In this figure the particle level set problem related to the topology change of an interface is represented. In blue the particles that define the interface are represented, whereas the interface itself is defined in red. In **A** the square before the topology change is reported whereas **B** reports the vector velocities in the system. In **C** and **D** the particles and the velocities after the topology change are represented. As it can be seen there are several particles that escape from the interface. This can results into several numerical and physical errors Osher et al. (2002).

$$\mathbf{n}(\phi) = \frac{\nabla\phi}{|\nabla\phi|}, \tag{26}$$

$$k_\gamma(\phi) = -\nabla \cdot \left(\frac{\nabla\phi}{|\nabla\phi|}\right). \tag{27}$$

This is one of the most important features of LSM. In fact, although it is not only easy to define the versor normal and the curvature, their computation allows to reach an incredible degree of accuracy, thanks to the high-order schemes that can be applied. These advantages come from the continuity of ϕ which also changes sign smoothly at the interface ($\phi = 0$).

The LSM is generally completed by one single momentum balance equation in which the properties of the fluid, namely density, $\rho(\phi)$, and viscosity, $\mu(\phi)$, are written in terms of the level set function, ϕ:

$$\rho(\phi)\left(\frac{\partial \mathbf{U}}{\partial t} + \mathbf{U}\cdot\nabla\mathbf{U}\right) = -\nabla p + \mu(\phi)\nabla^2\mathbf{U} + \gamma k_\gamma(\phi)\delta(\phi)\nabla\phi + \rho(\phi)\mathbf{g}. \tag{28}$$

The terms on the left-hand side of Eq. (28) represent accumulation and convective transport of momentum density, whereas the terms on the right-hand side represent the effect of pressure, viscous forces, interfacial tension forces and gravity. γ is the interfacial tension between phase 1 and 2.

$$\mathbf{U} = \begin{cases} \mathbf{U}_1 & \text{if} \quad \phi < 0 \\ \mathbf{U}_2 & \text{if} \quad \phi > 0, \end{cases} \tag{29}$$

$$\rho(\phi) = \rho_1 + (\rho_2 - \rho_1)H(\phi), \tag{30}$$

$$\mu(\phi) = \mu_1 + (\mu_2 - \mu_1)H(\phi), \tag{31}$$

where $H(\phi)$ is the Heaviside function defined as follows:

$$H(\phi) = \begin{cases} 0 & \text{if} \quad \phi < 0 \\ 1/2 & \text{if} \quad \phi = 0 \\ 1 & \text{if} \quad \phi > 0, \end{cases} \tag{32}$$

and where, as already explained, the indices 1 and 2 refer to the two phases involved. The LSM momentum equation can switch from one phase to another changing the viscosity and the density of the two fluids. Furthermore, the surface tension term is written as a delta function, leading the model to turn on automatically this contribution only on the interface. The Heaviside function keeps the density and viscosity change sharp, leading to high interface gradients. To avoid this it is necessary to smooth the interface by smoothing the Heaviside function.

A LSM simulation is usually constituted by the following steps:

1. Initialize $\phi(\mathbf{x}, 0)$ to be a signed distance for the interface to be captured.

2. Solve Eq. (24) and Eq. (28).

3. Reinitialize $\phi(\mathbf{x}, t)$.

4. Repeat step 2 and 3.

It is essential that the reinitialization step is performed after the level set evolution, in order to solve the momentum equation with a correct signed distance ϕ. In general, how often to reinitialize depends on how quickly the signed distance property of ϕ deteriorates. This depends on the phenomenon that one wants to simulate and on the numerical schemes used.

The performance of a LSM simulation is generally assessed by considering a number of validation tests that are employed as benchmark. In one of them, proposed by Enright et al. (2005), consists in considering a circle defining the interface between phase 1 and 2. Then the system undergoes a superimposed sinusoidal velocity that deforms the circle. This deformation continues for 4 s and then the sign of the velocity field is changed, the flow is reversed, and after 4 s one is expected to retrieve the original circle. One example is reported in Fig. 20.

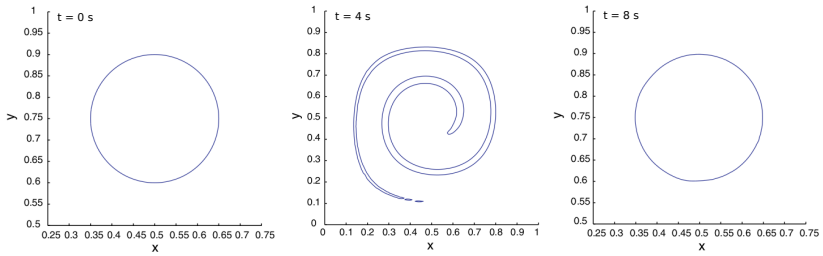

Figure 20: In this figure the evolution of a circular level set under a sinusoidal imposed velocity in a 126x126 grid is reported. The velocity field deforms the level set for $4s$ and then the simulation is rewound till the initial position inverting the velocity. The LSM implemented is performing well since the circle return to a shape very close to the original Enright et al. (2005).

3.3 Volume-of-Fluid

An alternative to the LSM is the Volume of Fluid (VOF) model, proposed by Noh and Woodward (1976); Hirt and Nichols (1981). Also here the discussion is limited to two-phase flows. The aim of the VOF is to be easy to implement, robust and fast, since it combines the governing equations into only one, in terms of a color function, C, which indicates the volume fraction of one phase in each cell:

$$C = \frac{\text{Volume of the chosen phase (e.g. phase 1)}}{\text{Total volume of the control volume}}. \tag{33}$$

It is possible to compute C for any one of the two phases as follows:

$$C(\mathbf{x}, t) = \begin{cases} 1, & \text{for a point inside fluid 1} \\ 0, & \text{for a point inside fluid 2} \\ 0 < C < 1, & \text{for a point inside a transitional area} \end{cases} \tag{34}$$

Once C is initialized, it is possible to compute the property of the multiphase system:

$$\rho(C) = C\rho_1 + (1 - C)\,\rho_2, \tag{35}$$

$$\mu(C) = C\mu_1 + (1 - C)\,\mu_2. \tag{36}$$

where the subscripts 1 and 2 indicate the properties of phase 1 and phase 2. The advection equation for C is defined as follows:

$$\frac{\partial C}{\partial t} + \mathbf{U} \cdot \nabla C = 0, \tag{37}$$

and the VOF model is completed by the momentum balance equation, obeying a formulation very similar to Eq. (28) of the LSM. Although the governing equations look very similar there are some important differences. The main difference is that in VOF the reconstruction of the interface is more difficult C is not continuous at the interface and several methods have been proposed Rudman (1997).

Simple line interface calculation (SLIC): The SLIC method Noh and Woodward (1976) represents the easiest way to perform the reconstruction. In this method the interface is approximated with a straight line parallel to one coordinate direction. This method is based on a direction-split algorithm. During each direction sweep, the interface is reconstructed only with the cell neighbors in the sweep direction. Since the method looks only to the neighbor in the flux direction, the same interface cell can be reconstructed in a different way for each direction sweep. The results are not very accurate, since it is random with the direction of the flow and it is difficult to represent it with high-order scheme. An examples of the SPLIC method is shown in Fig. 21.B and Fig. 21.C

Hirt-Nichols VOF: The method of Hirt and Nichols (1981) is the "original VOF" since it was the truly first VOF method developed. Similarly to the SLIC, the interface is reconstructed with a straight line parallel to one direction. However, the direction it is not chosen from the flux but from the normal direction of the interface, evaluating the magnitude of the normal components of the cell neighbors. The results obtained are generally more accurate than those obtained with SLIC method, even if it lacks accuracy, since, at least, the interface is reconstructed with the value of a neighbor only. An example is shown in Fig. 21.d.

Youngs' method: The method developed by Youngs Youngs (1982) improves what proposed by Noh and Woodward (1976); Hirt and Nichols (1981). The interface is still a straight line, but it is not forced to be parallel to the coordinates axes. The direction is obtain by the direction normal to the interface, but the normal is computed taking into account the color function of all the neighbors of the interface cells. An examples of the method of Youngs is shown in Fig. 21.E.

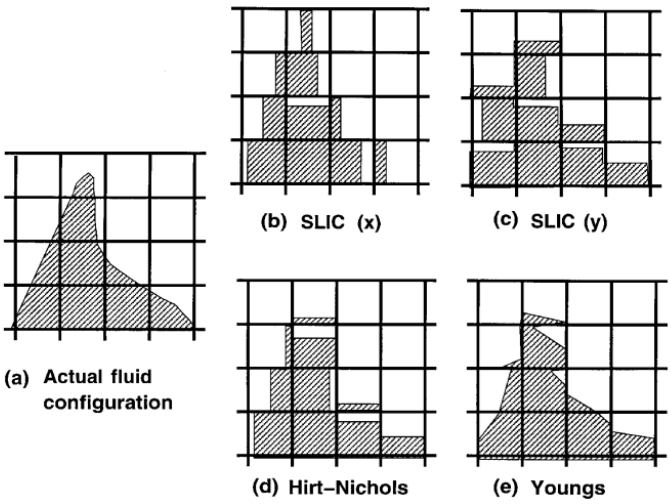

Figure 21: In this figure the results of different interface reconstruction for the configuration reported in (a) are represented. In (b) and (c) the results obtained with the SLIC approach are reported respectively for two different orientations. In (d) the result obtained with the method of Hirt and Nichols (1981) is reported. In (e) the reconstruction obtained with the method of Young Youngs (1982) is reported. It is clear how the method improves moving from (b) to (e)Rudman (1997).

Piecewise linear interface calculation (PLIC): The PLIC method goes beyond the work of Youngs (1982), since it was understood that the key factor is played by an accurate normal reconstruction. There are several methods to reconstruct properly the normal of the interface and here we report the method suggested by Rudman (1997) for a two dimensional space:

$$n^x_{i,j} = \frac{1}{h}\left(C_{i+1,j+1} + 2C_{i+1,j} + C_{i+1,j-1} - C_{i-1,j+1} - 2C_{i-1,j} - C_{i-1,j-1}\right), \tag{38}$$

$$n^y_{i,j} = \frac{1}{h}\left(C_{i+1,j+1} + 2C_{i,j+1} + C_{i-1,j+1} - C_{i+1,j-1} - 2C_{i,j-1} - C_{i-1,j-1}\right), \tag{39}$$

where the indices i and j indicate the x and y directions in a simple cartesian discretization. After the normal is computed and the average values of C in each cell is calculated, it is possible to calculate with good accuracy the position of the interface.

The performance of the different reconstruction methods briefly summarized here is assessed in Fig. 22, where the same test described in Fig. 20 is analyzed. Clearly the Youngs method shows the best performance which is however still not comparable with that of the LSM.In fact, the VOF model is more prone to suffer from issues caused by numerical diffusion, leading to an inaccurate evolution of the interface. It is important not to confuse the difference between "smooth interface" and the "diffusion of the interface". The first is a desirable property, since it allows for an easier computation of the surface properties, while the second artificially changes the interface thickness.

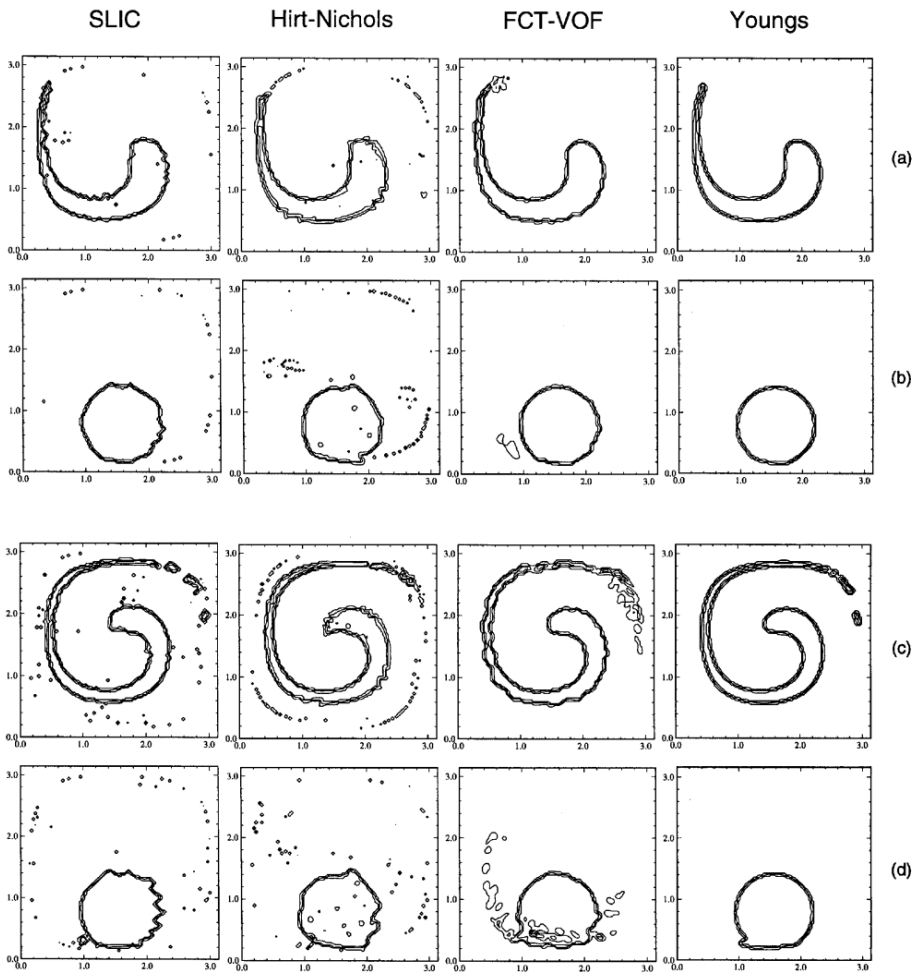

Figure 22: Results for an advection test on the different VOF methods. In the first column the results obtained with the SLIC method is represented. In the second, third and fourth column the Hirt-Nichols Hirt and Nichols (1981) method result, the FCT-VOF method of Rudman Rudman (1997) result and the method of Young Youngs (1982) result are respectively represented. From (a) to (d) different time steps of the simulations are reported. The test is the same presented in Fig. 20, based on a test case of Leveque LeVeque (1996). Rudman (1997).

3.4 Two-fluid Model

As already mentioned the LSM and the VOF model track the evolution of the interface, resulting in large computational costs. An interesting alternative is to forget about the interface and track instead the evolution of the multiphase system only in terms of the volume fractions of the involved phases. This is the basic assumption of the TFM and in what follows the discussion is limited to a two-phase system. The two involved phases are treated as interpenetrating continua with volume fractions that sum to unity: $\alpha_1+\alpha_2 = 1$. No information about the actual interface is tracked, the only known information is the amount of one phase with respect to the other. This implies that the effect of interfacial forces cannot be accounted for.

Different derivations of the TFM are reported in the literature based on volume-, time- or ensemble-averages. Here we refer to the work of Ishii and Mishima (1984) and of Marchisio and Fox (2013) for a model detailed discussion. In the final governing equations for the TFM we find the continuity equations for the two phases:

$$\frac{\partial}{\partial t}\left(\alpha_1\rho_1\right) + \nabla\cdot\left(\alpha_1\rho_1\mathbf{U}_1\right) = \Gamma_1, \tag{40}$$

$$\frac{\partial}{\partial t}\left(\alpha_2\rho_2\right) + \nabla\cdot\left(\alpha_2\rho_2\mathbf{U}_2\right) = \Gamma_2, \tag{41}$$

where Γ_1 and Γ_2 represent the mass transfer terms representing positive or negative generation for the two phases. Indeed: $\Gamma_1 + \Gamma_2 = 0$, to fulfill total mass conservation. In the case of disperse multiphase systems these terms refer to the already mentioned mechanisms of nucleation, growth and dissolution. The TFM is completed by the momentum balance equations for the two phases:

$$\frac{\partial}{\partial t}\left(\alpha_1\rho_1\mathbf{U}_1\right) + \nabla\cdot\left(\alpha_1\rho_1\mathbf{U}_1\mathbf{U}_1\right) = \\ -\alpha_1\nabla p_1 - \nabla\cdot\left[\alpha_1\left(\boldsymbol{\tau}_1+\boldsymbol{\tau}_{T1}\right)\right] + \alpha_1\rho_1\mathbf{g} + \Gamma_1\mathbf{U}_1 + \mathbf{M}_\mathrm{I}, \tag{42}$$

$$\frac{\partial}{\partial t}\left(\alpha_2\rho_2\mathbf{U}_2\right) + \nabla\cdot\left(\alpha_2\rho_2\mathbf{U}_2\mathbf{U}_2\right) = \\ -\alpha_2\nabla p_1 - \nabla\cdot\left[\alpha_2\left(\boldsymbol{\tau}_2+\boldsymbol{\tau}_{T2}\right)\right] + \alpha_2\rho_1\mathbf{g} + \Gamma_2\mathbf{U}_2 - \mathbf{M}_\mathrm{I}. \tag{43}$$

The terms appearing on the right-hand side represents the effect of pressure forces, of viscous and turbulent stresses, gravity and momentum coupling due to interfacial forces. Most of the terms appearing on the right-hand side need to be modeled, as any information concerning the interface is lost in the averaging procedure.

Self-interaction terms. There are several ways to describe the viscous stresses but for a Newtonian fluid the following constitutive equation is valid:

$$\boldsymbol{\tau}_k = -\mu_k\left(\nabla\mathbf{U}_k + \left(\nabla\mathbf{U}_k\right)^T\right) + \frac{2}{3}\mu_k\left(\nabla\cdot\mathbf{U}_k\right)\mathbf{I}, \tag{44}$$

with $k = 1, 2$ and where μ_k is the viscosity of the corresponding phase.

Momentum coupling. As mentioned, interfacial forces are exchanged between the involved phases, resulting in the phase coupling term, $\mathbf{M}_\mathrm{I}$, that is given by different contributions. In the case of disperse multiphase systems the most important is the drag force, described in Eq. (11) for one single bubble/droplet/particle. The resulting expression for the drag force in the phase momentum balance reads as follows:

$$\mathbf{M}_\mathrm{I} = -\alpha_1 \frac{3}{4} \frac{\rho_2 \mathrm{C_D}}{d} \mathbf{U}_\mathrm{s} |\mathbf{U}_\mathrm{s}| \tag{45}$$

where $\mathbf{U}_\mathrm{s} = \mathbf{U}_2 - \mathbf{U}_1$ is the already introduced slip velocity, namely the velocity difference between phase 1 and phase 2, and index 1 refers to the disperse phase and index 2 to the continuous phase.

Turbulence. There are several methods to deal with turbulence and in section we focus on the Reynolds-Averaged Navier-Stokes equations (RANS) approach. With this approach the turbulent stresses, $\boldsymbol{\tau}_{T1}$, and, $\boldsymbol{\tau}_{T2}$, are closed with an approximation similar to Eq. (44) with the molecular viscosity replaced with the turbulent viscosity. In the case of disperse multiphase system usually only the turbulent stresses in the continuous phase are considered, whereas those of the disperse phase are neglected. The most popular method to describe turbulence in the continuous phase, in the context of the RANS approach, is the k-ϵ model in which additional equations for the continuous phase turbulent kinetic energy and turbulent dissipation rate are solved:

$$\frac{\partial \alpha_2 k}{\partial t} + \nabla \cdot (\alpha_2 \mathbf{U}_2 k) - \nabla \cdot \left(\alpha_2 \frac{\nu_{\mathrm{t}2}}{\sigma_k} \nabla k \right) = \alpha_2 \left(G + \frac{P_{\mathrm{b},k}}{\rho_2} - \epsilon \right), \tag{46}$$

$$\frac{\partial \alpha_2 \epsilon}{\partial t} + \nabla \cdot (\alpha_2 \mathbf{U}_2 \epsilon) - \nabla \cdot \left(\alpha_2 \frac{\nu_{\mathrm{t}2}}{\sigma_\epsilon} \nabla \epsilon \right) = \alpha_2 \left[\left(C_{\epsilon,1} \frac{\epsilon}{k} G - C_{\epsilon,2} \frac{\epsilon^2}{k} \right) + P_{\mathrm{b},\epsilon} \right]. \tag{47}$$

where:

$$\nu_{t2} = C_\mu \frac{k_2^2}{\varepsilon_2}, \tag{48}$$

$$G = 2\nu_{\mathrm{t}2} \left(\nabla \mathbf{U}_2 : \nabla \mathbf{U}_2 \right), \tag{49}$$

$$P_{\mathrm{b},k} = C_\mathrm{b} \mathbf{M}_I^\mathrm{d} \cdot (\mathbf{U}_1 - \mathbf{U}_2), \tag{50}$$

$$P_{\mathrm{b},\epsilon} = C_\mathrm{bd} \alpha_1 \frac{k_1^{3/2}}{d}. \tag{51}$$

and where $\mathrm{C_b}$ varies from 0.02 to 0.75 while $\mathrm{C_{bd}}$ varies from 0.02 to 0.2. The high variability of these two parameters is due to the difficulties in the development of k-ε model for multiphase systems (Marchisio and Fox, 2007).

3.5 Mixture Model

As mentioned in the previous sections, in the case of relatively small Stokes numbers, the solution of a specific balance equation for the continuous and for the disperse phase is not necessary. In fact, under these conditions the disperse phase instantaneously adapts to the local value of the continuous phase. The problem can therefore be written in terms of

the mixture between the continuous and disperse phase. The mixture is usually defined in terms of its density:

$$\rho_{\mathrm{m}} = \rho_{\mathrm{c}}\alpha_{\mathrm{c}} + \rho_{\mathrm{d}}\alpha_{\mathrm{d}}, \tag{52}$$

which obeys the following equations:

$$\frac{\partial \rho_{\mathrm{m}}}{\partial t} + \nabla \cdot (\rho_{\mathrm{m}}\mathbf{U}_{\mathrm{m}}) = 0. \tag{53}$$

Another important property of the mixture is its velocity:

$$\mathbf{U}_{\mathrm{m}} = \rho_{\mathrm{c}}\alpha_{\mathrm{c}}\mathbf{U}_{\mathrm{c}} + \rho_{\mathrm{d}}\alpha_{\mathrm{d}}\mathbf{U}_{\mathrm{d}}, \tag{54}$$

whose transport equation can be obtained by summing the momentum balance equations for the two phases of the TFM:

$$\frac{\partial}{\partial t}(\rho_{\mathrm{m}}\mathbf{U}_{\mathrm{m}}) + \nabla \cdot (\rho_{\mathrm{m}}\mathbf{U}_{\mathrm{m}}\mathbf{U}_{\mathrm{m}}) = -\nabla p_{\mathrm{m}} - \nabla \cdot (\boldsymbol{\tau}_{\mathrm{m}} + \boldsymbol{\tau}_{\mathrm{Tm}}) + \rho_{\mathrm{m}}\mathbf{g}, \tag{55}$$

where all the properties refer to the mixture and where the mixture viscous stress reads as follows:

$$\boldsymbol{\tau}_{\mathrm{m}} = -\mu_{\mathrm{m}} \sum_{k=1}^{2} \left[\nabla \mathbf{U}_k + (\nabla \mathbf{U}_k)^{\mathrm{T}} - \frac{2}{3}\mathbf{I}(\nabla \cdot \mathbf{U}_k) \right], \tag{56}$$

the mixture turbulent stress as follows:

$$\boldsymbol{\tau}_{\mathrm{Tm}} = -\mu_{\mathrm{Tm}} \sum_{k=1}^{2} \left[\nabla \mathbf{U}_k + (\nabla \mathbf{U}_k)^{\mathrm{T}} - \frac{2}{3}\mathbf{I}(\nabla \cdot \mathbf{U}_k) \right] - \frac{2}{3}\rho_{\mathrm{m}} k_{\mathrm{m}} \mathbf{I}, \tag{57}$$

and where the molecular and turbulent mixture viscosities are calculated as follows:

$$\mu_{\mathrm{m}} = \sum_{k=1}^{2} \alpha_k \mu_k, \tag{58}$$

$$\mu_{\mathrm{Tm}} = \sum_{k=1}^{2} \alpha_k \mu_{\mathrm{T}k}. \tag{59}$$

These equation can be solved if the velocity of the continuous phase, $\mathbf{U}_2 = \mathbf{U}_{\mathrm{c}}$, and of the disperse phase, $\mathbf{U}_1 = \mathbf{U}_{\mathrm{d}}$, are calculated from the mixture velocity, $\mathbf{U}_{\mathrm{m}}$. One very simple approach is to assume a constant slip velocity:

$$\mathbf{U}_{\mathrm{s}} = \mathbf{U}_2 - \mathbf{U}_1, \tag{60}$$

which can be used a model parameter. Alternatively a more rigorous approach can be used by considering instantaneous equilibrium between the forces acting on the elements of the disperse phase.

4 Conclusions and perspective

In these notes after having classified the type of multiphase systems encountered in nature and engineering applications a number of computational models for their simulation has been discussed. They are classified by the degree of accuracy and associated computational cost.

Starting from the most accurate and moving on to the less accurate we have:

- molecular dynamics models: the molecular details for the involved phases are explicitly described
- direct numerical simulation: continuum model in which the interfaces are tracked directly
- probability density function methods: the interface is not tracked but the properties of the multiphase system are expressed in terms of distribution function
- moment methods: the multiphase system is described in terms of the moments of the above-mentioned distributions

Guidelines for selecting the most appropriate multiphase computational models are also discussed and eventually some of them are described with more details.

References

Bazzano, M., Marchisio, D., Sangermano, M., Wörner, M., and Pisano, R. (2019). A molecular dynamics approach to nanostructuring of particles produced via aerosol cationic photopolymerization. *Chemical Engineering Science*, 195:1021–1027.

Bird, B. R., Stewart, W. E., and Lightfoot, E. N. (1960). *Transport Phenomena*. John Wiley and Sons.

Boccardo, G., Buffo, A., and Marchisio, D. (2019a). Simulation of mixing in structured fluids with dissipative particle dynamics and validation with experimental data. *Chemical Engineering and Technology*, 42(8):1654–1662.

Boccardo, G., Sethi, R., and Marchisio, D. (2019b). Fine and ultrafine particle deposition in packed-bed catalytic reactors. *Chemical Engineering Science*, 198:290–304.

Castellano, S., Carrillo, L., Sheibat-Othman, N., Marchisio, D., Buffo, A., and Charton, S. (2019). Using the full turbulence spectrum for describing droplet coalescence and breakage in industrial liquid-liquid systems: Experiments and modeling. *Chemical Engineering Journal*, 374:1420–1432.

Clift, R., Grace, J. R., and Weber, M. E. (1978). *Bubbles, Drops, and Particles*. Academic Press.

Di Pasquale, N., Marchisio, D., Barresi, A., and Carbone, P. (2014). Solvent structuring and its effect on the polymer structure and processability: The case of water-acetone polycaprolactone mixtures. *Journal of Physical Chemistry B*, 118(46):13258–13267.

Drew, D. A. and Passman, S. L. (1999). *Theory of Multicomponent Fluids*. Springer, New York.

Droghetti, H., Pagonabarraga, I., Carbone, P., Asinari, P., and Marchisio, D. (2018). Dissipative particle dynamics simulations of tri-block co-polymer and water: Phase diagram validation and microstructure identification. *Journal of Chemical Physics*, 149(18).

Enright, D., Losasso, F., and Fedkiw, R. (2005). A fast and accurate semi-lagrangian particle level set method. *Computers and Structures*, 83:479–490.

Frungieri, G., Boccardo, G., Buffo, A., Marchisio, D., Karimi-Varzaneh, H., and Vanni, M. (2020). A cfd-dem approach to study the breakup of fractal agglomerates in an internal mixer. *Canadian Journal of Chemical Engineering*.

Gemello, L., Plais, C., Augier, F., and Marchisio, D. (2019). Population balance modelling of bubble columns under the heterogeneous flow regime. *Chemical Engineering Journal*, 372:590–604.

Hirt, C. W. and Nichols, B. D. (1981). Volume of fluid (vof) method for the dynamics of free boundaries. *Journal of Computational Physics*, 39:201–225.

Ishii, M. and Mishima, K. (1984). Two-fluid model and hydrodynamic constitutive relations. *Nuclear Engineering and Design*, 82:107–126.

Karimi, M., Marchisio, D., Laurini, E., Fermeglia, M., and Pricl, S. (2018). Bridging the gap across scales: Coupling cfd and md/gcmc in polyurethane foam simulation. *Chemical Engineering Science*, 178:39–47.

Lavino, A., Banetta, L., Carbone, P., and Marchisio, D. (2018). Extended charge-on-particle optimized potentials for liquid simulation acetone model: The case of acetone-water mixtures. *Journal of Physical Chemistry B*, 122(20):5234–5241.

Lavino, A., Carbone, P., and Marchisio, D. (2020). Martini coarse-grained model for polycaprolactone in acetone-water mixtures. *Canadian Journal of Chemical Engineering*.

Lavino, A., Di Pasquale, N., Carbone, P., and Marchisio, D. (2017). A novel multiscale model for the simulation of polymer flash nano-precipitation. *Chemical Engineering Science*, 171:485–494.

LeVeque, R. J. (1996). High-resolution conservative algorithms for advection in incompressible flow. *SIAM Journal on Numerical Analysis*, 33(2):627–665.

Li, D., Marchisio, D., Hasse, C., and Lucas, D. (2019). Comparison of eulerian qbmm and classical eulerian–eulerian method for the simulation of polydisperse bubbly flows. *AIChE Journal*, 65(11).

Li, D., Marchisio, D., Hasse, C., and Lucas, D. (2020). twowaygpbefoam: An open-source eulerian qbmm solver for monokinetic bubbly flows. *Computer Physics Communications*, 250.

Li, D., Wei, Y., and Marchisio, D. (2021). Qeefoam: A quasi-eulerian-eulerian model for polydisperse turbulent gas-liquid flows. implementation in openfoam, verification and validation. *International Journal of Multiphase Flow*, 136.

Marcato, A., Boccardo, G., and Marchisio, D. (2021). A computational workflow to study particle transport and filtration in porous media: Coupling cfd and deep learning. *Chemical Engineering Journal*, 417.

Marchisio, D. L. and Fox, R. O. (2007). *Multiphase reacting flows: modelling and simulation*. Springer-Verlag Wien.

Marchisio, D. L. and Fox, R. O. (2013). *Computational Models for Polydisperse Particulate and Multiphase Systems*. Cambridge University Press.

Monahan, S. M., Vitankar, V. S., and Fox, R. O. (2005). CFD predictions of flow-regime transitions in bubble columns. *AIChE Journal*, 51:1897–1923.

Noh, W. F. and Woodward, P. (1976). *SLIC (Simple Line Interface Calculation)*. Springer Berlin Heidelberg, Berlin, Heidelberg.

Osher, S., Sethian, J., and Fedkiw, R. P. (2002). *Level Set Methods and dynamiciImplicit surfaces*. Springer-Verlag.

Osher, S. and Sethian, J. A. (1988). Fronts propagating with curvature-dependent speed: Algorithms based on hamilton-jacobi formulations. *Journal of Computational Physics*, 79(12).

Pasquino, R., Droghetti, H., Carbone, P., Mirzaagha, S., Grizzuti, N., and Marchisio, D. (2019). An experimental rheological phase diagram of a tri-block co-polymer in water validated against dissipative particle dynamics simulations. *Soft Matter*, 15(6):1396–1404.

Passalacqua, A., Laurent, F., Madadi-Kandjani, E., Heylmun, J., and Fox, R. (2018). An open-source quadrature-based population balance solver for openfoam. *Chemical Engineering Science*, 176:306–318.

Pollack, M., Pütz, M., Marchisio, D., Oevermann, M., and Hasse, C. (2019). Zero-flux approximations for multivariate quadrature-based moment methods. *Journal of Computational Physics*, 398.

Prospetti, A. and Grétar, T. (2007). *Computational Methods for Multiphase Flow*. Cambridge University Press.

Rudman, M. (1997). Volume-tracking methods for interfacial flow calculations. *International Journal For Numerical Methods in Fluids*, 24:671–691.

Salenbauch, S., Hasse, C., Vanni, M., and Marchisio, D. (2019). A numerically robust method of moments with number density function reconstruction and its application to soot formation, growth and oxidation. *Journal of Aerosol Science*, 128:34–49.

Sankaranarayanan, K. and Sundaresan, S. (2002). Lift force in bubbly suspensions. *Chemical Engineering Science*, 57:3521–3542.

Shiea, M., Buffo, A., Baglietto, E., Lucas, D., Vanni, M., and Marchisio, D. (2019). Evaluation of hydrodynamic closures for bubbly regime cfd simulations in developing pipe flow. *Chemical Engineering and Technology*, 42(8):1618–1626.

Shiea, M., Buffo, A., Vanni, M., and Marchisio, D. (2020). Numerical methods for the solution of population balance equations coupled with computational fluid dynamics. *Annual Review of Chemical and Biomolecular Engineering*, 11:339–366.

Tronci, G. (2021). *CFD study of the bottling process with carbonated soft drinks*. Ph.d. thesis, Politecnico di Torino.

Youngs, D. L. (1982). *Time-dependent multi-material flow with large fluid distortion*. Academic Press.